6745

222

676158

TECHNICAL REPORT NO. 10023 (Final)

THE EFFECT OF LEAD ON MICRO-CRACK INITIATION AND PROPAGATION IN ALLOY STEELS

FINAL REPORT PHASE I

PART B: A FRACTOGRAPHIC STUDY OF LEADED 4145 STEEL TESTED AT ELEVATED TEMPERATURES

TECHNICAL LIBRARY
REFERENCE COPY

Distribution of This Document is Unlimted

by R. Zipp, Wm. R. Warke, and N. N. Brever
ILLINOIS INSTITUTE OF TECHNOLOGY

Date: August 1968

Contract No. DA-20-113-AMC-10820(T)

TACOM

VEHICULAR COMPONENTS & MATERIALS LABORATORY

U.S. ARMY TANK AUTOMOTIVE COMMAND Warren, Michigan

20040113037

The findings in this report are not to be construed as an Official Department of the Army position, unless so designated by other authorized documents.

Distribution of this document is unlimited.

The citation of commercial products in this report does not constitute an official indorsement or approval of such products.

Citation of equipment in this report does not constitute an official indorsement or approval of the use of such commercial hardware.

Destroy this report when it is no longer needed. Do not return it to the originator.

THE EFFECT OF LEAD ON MICRO-CRACK INITIATION AND PROPAGATION IN ALLOY STEELS

Final Report - Phase I

Part B

A FRACTOGRAPHIC STUDY OF LEADED 4145 STEEL TESTED AT ELEVATED TEMPERATURES

by

Richard Zipp, William R. Warke, and Norman N. Breyer

August 1968

Contract No. DA-20-113-AMC-10820(T)
U. S. Army Tank-Automotive Command
Warren, Michigan 48090

Distribution of this document is unlimited.

Department of Metallurgical Engineering
Illinois Institute of Technology
Chicago, Illinois 60616

ABSTRACT

It has been found that a 4145 steel containing 0.3% lead suffers a loss in ductility when tensile tested between 400°F and 900°F. A visual analysis of the fractured surfaces from both leaded and non-leaded tensile specimens was performed at various ultimate strength levels from 120 KSI to 240 KSI and the fractures were classified into five types.

An electron microscope fractographic study was made on the five fracture types. Fractographs taken from Type A fractures (R.T. to 400°F) showed that fracture by microvoid coalesence ("dimpled rupture") typified the entire fracture surface. Type B fractures (400°F to 600°F) were characterized by a mixture of intergranular regions in an otherwise transgranular failure. Each group of intergranular grain facets contained an inclusion. For a Type C fracture (600°F to 650°F) replicas taken from a cluster of small "fish eyes" showed both intergranular and transgranular modes of failure. Again, inclusions were present on the intergranular grain facets. A type D fracture (650°F to 900°F) was almost 100% intergranular at the origin of the single flat "fish eye." The per cent intergranular decreased as the crack grew until it was 100% transgranular near the extremity of the fracture at the far side of the "fish eye." Once again inclusions were present on the intergranular facets. Due to the fact that the Type E fracture occurs at high temperature (above 900°F), the surfaces were badly oxidized but appear to have been formed by a dimpled rupture process.

The association of inclusions with the intergranular fracture regions was deemed significant since the lead was always found in an envelope surrounding the inclusions. The results of this study are compatible with a "liquid metal embrittlement" interpretation of the loss in ductility at elevated temperature.

FOREWORD

This report is Part B of the Final Report, Phase I. The properties of leaded and non-leaded 4145 steel at strength levels from 120 to 240 ksi had been determined in the temperature range from room temperature to 900°F and were reported in Part A of the Final Report, Phase I. This part of the final report further substantiates the mechanism proposed to account for the embrittling effects of lead upon steels. Both macrofractography and electron microscope fractography have been utilized to examine the fracture surfaces of the tensile specimens tested in Part A of the program. This study amplifies the proposed mechanism. The program was authorized by the U. S. Army Tank Automotive Command (TACOM), Warren, Michigan under Contract No. DA-20-113-AMC-10820(T). Technical administration of the contract was the responsibility of V. H. Pagano, Chief, Metals Branch, Materials Laboratory, VCML, TACOM. The TACOM project engineer was C. J. Kropf.

TABLE OF CONTENTS

	Page No.
1. INTRODUCTION	1
1.1 The Problem	1
1.2 Background	1
2. OBJECTIVE	5
3. SUMMARY	5
4. CONCLUSIONS	6
5. RECOMMENDATIONS	6
6. EXPERIMENTS AND RESULTS	6
6.1 Materials and Experimental Techniques	6
6.2 Data and Results	7
6.2.1 Macroscopic Visual Analysis	7
6.2.2 Microscopic Analysis Using the Electron Microscope	10
6.2.2.1 High Strength Leaded Material	10
6.2.2.2. Low Strength Leaded Material	12
6.2.2.3. High and Low Strength Non-Leaded Material	13
7. DISCUSSION	13
BIBLIOGRAPHY	17
APPENDIX A ENGINEERING TENSILE PROPERTY CURVES	46
APPENDIX B PROBE WORK	59
DISTRIBUTION LIST	61
DD FORM 1473	65

LIST OF TABLES

Table Page No.

1. Test Temperatures at Which Each Fracture Type Occurred for Leaded and Non-Leaded Steel Specimens at Various Strength Levels 18

LIST OF FIGURES

Figure		Page No.
1	Engineering Tensile Properties of Non-Leaded N20 Material	19
2	Engineering Tensile Properties of Leaded L20 Material . . .	20
3	Transgranular Fracture by Microvoid Coalescence ("Dimpled Rupture"). 8,000X	21
4	"River Markings" that Characterize Transgranular Fracture by Cleavage. 6,000X	22
5	"Striation" that Characterize Transgranular Fracture by Cleavage. 6,000X	22
6	"Rock Candy" Appearance of an Intergranular Fracture Without Microvoid Coalescence	23
7	Classification of Longitudinal Tensile Specimen's Fracture Surface	24
8	Type A Fracture. Directly Parallel to Axis of Tensile Specimen. 10X	25
9	Type B Fracture. Directly Parallel to Axis of Tensile Specimen. 10X	26
10	a. Type C Fracture. Axis of Tensile Specimen Rotated 45° to Axis of Camera Lens. 10X	27
	b. High Magnification Photograph of the Golden Brown "Fish Eyes" Taken from a Type C Fracture. 500X . .	28
11	Type D Fracture. Directly Parallel to Axis of Tensile Specimen. 10X	29
12	Type E Fracture. Directly Parallel to Axis of Tensile Specimen. 10X	30

LIST OF FIGURES (Cont'd)

Figure		Page No.
13	Engineering Tensile Properties of Non-Leaded N-20 Material with Fracture Type Designation Indicated Adjacent to the Corresponding Points on the Reduction of Area Curve	31
14	Engineering Tensile Properties of Leaded L-20 Material with the Fracture Type Designation Indicated Adjacent to the Corresponding Points on the Reduction of Area Curve	32
15	Fibrous Center Region for a Type A Fracture Showing a Complete Transgranular Mode of Failure. 8,000X . . .	33
16	Radial Shear Region for a Type A Fracture Showing a Complete Transgranular Mode of Failure. 8,000X . . .	33
17	Shear Lip for a Type A Fracture Showing a Complete Transgranular Mode of Failure. 8,000X	34
18	a. Transgranular Fracture for a Type E Fracture in the Form of "Oxidized Dimples." 3,000X	35
	b. Transgranular Fracture for a Type E Fracture in the Form of "Oxidized Dimples." 3,000X	35
19	a. Primarily Intergranular Fracture for a Type B Fracture. 3,000X	36
	b. Primarily Intergranular Fracture for a Type B Fracture. 3,000X	36
20	a. Region Showing Both an Intergranular and a Transgranular Mode of Failure for a Type B Fracture. 3,000X	37
	b. Region Showing Both an Intergranular and a Transgranular Mode of Failure for a Type B Fracture. 3,000X	37

LIST OF FIGURES (Cont'd)

Figure		Page No.
21	a. Region Showing Both an Intergranular and a Transgranular Mode of Failure for a Type C Fracture Taken from a Cluster of Small "Fish Eyes." 3,000X . .	38
	b. Region Showing Both an Intergranular and a Transgranular Mode of Failure for a Type C Fracture Taken from a Cluster of Small "Fish Eyes." 3,000X . .	38
22	Schematic Drawing of Type D Fracture	39
23	a. Origin of Fracture Showing a Complete Intergranular Mode of Failure. 3,000X	40
	b. Origin of Fracture Showing a Complete Intergranular Mode of Failure. 3,000X	40
24	Intergranular and Transgranular Fracture Located in the Intermediate Region. 3,000X	41
25	Almost Completely Transgranular Fracture Located in the Outer Region. 8,000X	41
26	Inclusion Located on Intergranular Grain Facet for a Type D Fracture	42
27	Visual Estimation of Per Cent Intergranular as a Function of Crack Length for a Type D Fracture	43
28	Fractograph of Type B Fracture Taken from a Low Strength Material	44
29	Fractograph of Type C Fracture Taken from a Low Strength Material	44
30	Origin of Low Strength Type D Fracture Showing an Intergranular Mode of Failure	45
1A	Engineering Tensile Properties of Non-Leaded N-12 Material	47

LIST OF FIGURES (Cont'd)

Figure		Page No.
2A	Engineering Tensile Properties of Leaded L-12 Material . .	48
3A	Engineering Tensile Properties of Non-Leaded N-14 Material	49
4A	Engineering Tensile Properties of Leaded L-14 Material . .	50
5A	Engineering Tensile Properties of Non-Leaded N-16 Material	51
6A	Engineering Tensile Properties of Leaded L-16 Material . .	52
7A	Engineering Tensile Properties of Non-Leaded N-18 Material	53
8A	Engineering Tensile Properties of Leaded L-18 Material . .	54
9A	Engineering Tensile Properties of Non-Leaded N-22 Material	55
10A	Engineering Tensile Properties of Leaded L-22 Material . .	56
11A	Engineering Tensile Properties of Non-Leaded N-24 Material	57
12A	Engineering Tensile Properties of Leaded L-24 Material . .	58
1B	Inclusion Detected by Back Scattered Electrons	60
2B	Kα Radiation Revealing the Presence of Manganese in the Inclusion	60
3B	Kα Radiation Revealing the Presence of Sulfur in the Inclusion	60
4B	Mα Radiation Revealing the Presence of Lead in the Inclusion	60

Section 1

INTRODUCTION

1.1 THE PROBLEM

Mostovoy and Breyer investigated a 4145 steel with 0.3 per cent lead and determined that a severe loss in ductility occurs upon testing between 400°F and 900°F, and hypothesized that this phenomenon is caused by liquid metal embrittlement due to the lead (melting point of 621°F).[1*] This hypothesis also incorporates an explanation for this loss in ductility below the melting point of lead and the return of ductility above 900°F which is based upon the transport of the lead atoms to the crack tip as a vapor. If the hypothesis is correct, it would be anticipated that the embrittlement would occur by an intergranular fracture mode and that a fractographic study would support or deny the proposed hypothesis.

1.2 BACKGROUND

Mostovoy and Breyer investigated the tensile properties for 4145 leaded and non-leaded steel as a function of test temperature.[1] The ultimate strengths of the materials used varied from 120 ksi to 240 ksi in increments of 20 ksi. The trend of this data is exemplified by Figures 1 and 2 for a high strength material (200 ksi ultimate). Figure 1 (the non-leaded material) shows that there was no major loss in ductility over the range of test temperatures, while Figure 2 (the leaded material) shows that there was a severe loss in ductility between 400°F and 900°F. This type of behavior is typical of all the strength levels tested. At lower levels the leaded material, however, did not exhibit a total loss of ductility as measured by the reduction of area. Instead a finite minimum reduction of area occurred. Thus, the embrittlement

---

* For all numbered references, see bibliography.

takes place between 400°F and 900°F for all strength levels of leaded material although it is more severe for the higher strength material.

The tensile specimens tested by Mostovoy and Breyer and which yielded the data shown in these ductility curves were also the subject of the present fracture analysis. Examination of the fracture surface is one of the most important ways to gain an insight into the mechanics of the various fracture modes. Low magnification observations of fracture surfaces have for a long time aided metallurgists in their fracture analyses.[2] The chevron markings of brittle fractures and the concentric growth rings of fatigue are examples of the characteristics revealed by low-power optical microscopy in the study of fracture surfaces. Recently, however, a high magnification means of investigation has been added with the advent of the electron microscope. Because of its large depth of field and high resolving power, this instrument allows high magnification examination of areas of irregular contour.

The large depth of field which can be obtained with the electron microscope allows vertical height differences on the fracture surface to be analyzed. These height differences can reveal interesting facts about the mode of fracture. For example, if three flat facets meeting at a point are observed on the fracture surface, one would probably conclude that this region of the fracture is intergranular because the triple point represents a region where the grains are joined.

The high resolving power of the electron microscope allows horizontal differences on the fracture surface to be evaluated. This evaluation can also reveal pertinent information about the mode of fracture. For example, the electron microscope reveals the "striations" which are characteristic of a fatigue failure and can be used as a quantitative measure of the microscopic crack propagation rate. It should be remembered, however, that while resolving power of the electron microscope increases with increasing magnification, the depth of field decreases.

The main disadvantage of the electron microscope is that the fracture itself is not directly observed.[3] Instead, very thin replicas of the fracture surface must be prepared and transferred into the microscope for study. These replicas are usually made by the one stage or two stage method. Since the one stage replicating technique requires that the fracture surface be destroyed during replicating, only the two stage method will be explained in the Material and Experimental Techniques section of this report.

Fractures should be studied using the different optical techniques and electron fractography does not replace optical microscopy or observations with the unaided eye. An electron fractograph by itself, for instance, cannot always indicate whether a macroscopic fracture was ductile or brittle. Electron fractography, then, should be considered as a complementary tool for fracture studies and failure analysis.

In order to evaluate these fractures, it is necessary to understand what type of fracture surface would be expected to result from tensile testing a heat treated steel. According to Larson and Carr,[4] the resulting fracture surface from a ductile steel is composed of a fibrous central region, a radial shear intermediate region, and a shear lip outer region. The fibrous central region is composed of circumferential ridges which surround the origin of the fracture. The origin can easily be distinguished from the rest of the fibrous zone because it is a conical shaped area. The radial shear region is located between the fibrous area and shear lip and it is characterized by radial markings which represent the transition from slow to fast fracture. The shear lip zone forms the outer perimeter of the fracture and represents the region where the final mode of failure is shear on a 45° plane. The size of each of the three previously described zones is temperature dependent. As the temperature is increased, the size of the fibrous and shear lip zones increases at the expense of the radial shear zone.

Before presenting fractographs taken with the electron microscope, it is first necessary to understand the characteristics of fractures as seen with this microscope.[5-9] All fractures may be divided into two broad categories according to fracture path: transgranular (through the grains), and intergranular (along the grain boundaries). The mechanisms by which the fracture propagates during transgranular crack growth are: 1) microvoid coalescence, 2) cleavage, and 3) fatigue; while during intergranular crack propagation the mechanisms are: 1) grain boundary separation with microvoid coalescence, and 2) grain boundary separation without microvoid coalescence.

In transgranular fracture by microvoid coalescence, the microvoids are probably nucleated at grain boundaries, sub-grain boundaries, second phase particles, inclusions, or any site where there may be a strain discontinuity. These microvoids grow, coalesce by necking of the walls between

adjacent voids, and eventually form a fracture surface as the stress increases. The fracture surface reveals many cup-like depressions or dimples (Figure 3) that result from the microvoid coalescence.

The principal stresses acting on the fracture surface influence the shape of the dimples. Fracture under conditions of uniaxial tension usually result in the formation of equiaxed dimples on the fracture surface. Failures caused by shear stress or tensile stresses that initiate a tearing fracture mode will produce "parabolically" shaped dimples, or "elongated" dimples. If the failure is caused by shear stresses, the dimples will be pointing in opposite directions on the matching fracture surfaces; while if tensile tear is the cause, the dimples will be pointing in the same direction on the matching fracture surfaces.

In transgranular fracture by cleavage, fracture takes place along crystallographic planes within a grain. Because the grains are randomly oriented with respect to one another, a cleavage crack propagating through one grain will probably have to change direction as it crosses into another grain or sub-grain boundary. The fracture surface consists of flat facets, which contain characteristic markings known as "river markings" (Figure 4). These "river markings" are actually steps on the fracture surface and represent a crack propagation of two slightly different levels. The origin of the fracture may be found by tracing these markings "upstream."

Transgranular fracture by fatigue is characterized by the appearance of striations normal to the direction of crack propagation on the fracture surface (Figure 5). The striations are due to the cyclic or repetitive loading which causes fracture. The actual mechanism of crack nucleation is believed to involve slip plane fracture caused by repetitive reversing of the operative slip systems in the metal, while the mechanism of crack propagation is believed to involve the formation of troughs at the tip of the fatigue crack due to cyclic plastic deformation accompanied by alternate blunting and sharpening of the crack tip.

The presence of grain boundary precipitates, grain boundary weakness, and interaction between the grain boundary and the environment are conditions that normally lead to intergranular fracture. The only basic difference between grain boundary separation with microvoid coalescence and separation without coalescence is the appearance of dimples on those fractures that fail by micro-

void coalescence. Intergranular fracture without microvoid coalescence is characterized by its "rock candy" appearance (Figure 6). Note that the fracture has a three-dimensional appearance; if stereographic photographs are taken of this same area, the fracture would have a "mountain-like" appearance. The fracture grain facets do not have any dimples, which shows that the fracture took place without microvid coalescence.

Section 2

OBJECTIVE

The overall objective of the program is to provide design and materials engineers with information regarding the effect of lead upon the mechanical properties of alloy steels. This objective includes the influence of the intrinsic strength upon mechanical properties of leaded steels and is aimed at understanding unexplained catastrophic failures which have been encountered during the processing and subsequent service. Frequently contractors and subcontractors producing tank-automotive equipment request permission to use leaded steels for their improved machinability. The design agency can now realistically consider the possibilities of part failures due to the brittleness introduced with the lead additive and make judgments as to equivalency and/or increase inspection requirements.

Section 3

SUMMARY

This report, Part B, verifies the embrittling effects of lead upon high strength steels. Fractographic studies reveal that the embrittlement in the temperature range between 400°F and 900°F for leaded 4145 steel is associated with inclusion sites. Because the lead exists as an envelope around the inclusion, the fractographic analysis of the fracture surface is consistent with the vapor transport mechanism proposed in Part A.

Section 4

CONCLUSIONS

1) Because of the observed intergranular fracture behavior it was concluded that some form of liquid metal embrittlement was associated with the loss in ductility between 400°F and 900°F for leaded 4145 steel.

2) The results of this fractographic analysis are consistent with the proposed vapor transport mechanism of embrittlement. The intergranular cracking was associated with inclusions and increased in extent with increasing temperature in the range 400°F to 650°F where transport in the vapor phase can be reconciled.

Section 5

RECOMMENDATIONS

It is recommended that the substitution of leaded alloy steel not be made for the non-leaded variety as a routine basis. Consideration of the part and the intensive inspection procedures to insure the freedom from cracks are mandatory. Although only one steel analysis at one lead level has been tested to date in the program the continuing investigation which encompasses other steel types and lead levels as well as other testing methods will aid the materials engineer in specifying alloy steels.

Section 6

EXPERIMENTS AND RESULTS

6.1 MATERIALS AND EXPERIMENTAL TECHNIQUES

The leaded and non-leaded 4145 steel tensile specimens for the present study were those previously tested.[1] Both the non-leaded and leaded specimens had been fractured at temperatures ranging from 72°F to 900°F. The room temperature ultimate tensile strength levels for both materials varied from 120 ksi to 240 ksi in increments of 20 ksi.

These specimens were examined visually under a stereo binocular microscope at 7X to 30X magnifications. The results that were obtained from this analysis were recorded by classifying the different fracture types observed and by taking macrophotographs of selected fracture surfaces at 10X with a Linhosf camera.

The surfaces of selected fractures were replicated with cellulose acetate tape and shadowed for electron microscopic examination. The replication technique consisted of wetting the tape with acetone for about eight seconds and pressing it firmly with an eraser onto the fractured surface for about ten seconds. The plastic replica was then allowed to dry on the fractured surface for fifteen minutes. Next, the replica was stripped from the specimen and placed in an evacuated bell jar to be shadowed with platinum-carbon. A backing layer of carbon was also deposited. After removal from the vacuum evaporator, selected areas of interest were sectioned from the replica and placed on electron microscope specimen grids. The plastic portion of the shadowed replica was dissolved by washing, leaving only a platinum-carbon replica for examination under the electron microscope. Magnifications in the range 3,000X to 10,000X were found adequate for this program.

6.2 DATA AND RESULTS

6.2.1 MACROSCOPIC VISUAL ANALYSIS

The fracture surfaces of the longitudinal tensile specimens were classified by visual analysis into five categories (A, B, C, D, E) as shown by the schematic sketches of Figure 7 and the macrophotographs of Figures 8 through 12. Type A, shown in Figure 7a and Figure 8, was a low temperature cup and cone fracture consisting of a fibrous central region, a radial shear intermediate region, and a shear lip outer region. In a Type B fracture, shown in Figure 7b and Figure 9, the entire flat fracture surface was very rough, except for very small shear lips, and exhibited a golden brown color. Type C fractures, shown in Figure 7C and Figure 10a, occurred on a plane inclined at about a 45° angle to the axis of the tensile specimen, i.e., they were generally shear fractures. The fracture surfaces of Type C fractures were covered with an adherent blue oxide film. However, there were a number of small flat circular irregularities oriented normal to the tensile axis along the inclined fracture surfaces. These regions resembled

small "fish eyes" and appeared very similar to the Type B fractures. These irregularities were easy to locate on the fracture surface because of their golden brown color, as can be seen in Figure 10b which shows one of them at 500X. In Type D, shown in Figure 7d and Figure 11, an off-center flat region was surrounded by a shear lip. It appeared that one large fish eye formed at or near the specimen surface and grew until the remaining section fractured in shear. The color differences were not as clear as those outlined above, but some color and texture gradations could be seen across the fish eye. Finally, Type E, shown in Figure 7e and Figure 12, was a high temperature cup and cone fracture. The center and intermediate regions were fibrous in nature; the outer region was a shear lip fracture.

Each fractured tensile specimen was classified as Type A, B, C, D, or E; and each was associated with a point on one of the reduction of area versus test temperature curves plotted by Mostovoy and Breyer for both leaded and non-leaded material. A typical pair of these curves is shown in Figure 13 for non-leaded, 200 ksi ultimate, material and in Figure 14 for leaded, 200 ksi ultimate, material. The corresponding engineering tensile property curves for the other strength levels can be found in Appendix A. In these figures the "fracture type" designation is indicated adjacent to the corresponding points on the reduction of area curves. For the non-leaded, 200 ksi material, a Type A fracture occurred at room temperature and at 400°F, while Type E occurred at 600°F, 700°F, 800°F, and 900°F. Note that for the non-leaded material, fracture Types B, C, and D did not occur and that no embrittlement existed over the entire temperature range. From the shape of the ductility curve for leaded 200 ksi material, it is seen that a severe embrittlement took place between 400°F to 900°F and that fracture Types B, C, and D were associated with this embrittlement. Between room temperature and 400°F, Type A fractures took place, and at temperatures above 900°F, Type E fractures occurred. The Type B fracture seemed to be associated with the onset of embrittlement, while the Type C fracture took place when the embrittlement became more severe. Type D fractures were obtained when minimum ductility occurred for the strength level being tested. In the case of the 200 ksi material, Type D fractures exhibited a complete loss of reduction of area. For the lower strength level material, the minimum ductility and Type D fracture took place with a measurable value for reduction of area; nevertheless, the shape of the reduction of area versus test temperature curve was similar to that for the high strength material.

The remaining strength levels for the leaded and non-leaded material had similarly shaped ductility curves, as can be seen in Appendix A. The fracture type was correlated for the various temperatures and strength levels and is presented in tabular form in Table 1. The material in this table is in a coded form, in which the letters L and N designate the leaded or non-leaded material, respectively, and the number pertains to the ultimate strength level in 10,000 psi multiples. For example, the code N-16 indicates a non-leaded, 160 ksi ultimate tensile strength material, while L-22 corresponds to leaded, 220 ksi ultimate tensile strength material.

Several general conclusions regarding the fracture of non-leaded steels can be drawn from an examination of Table 1 and Figure 13. Type A fractures occurred between room temperature and about 550°F and Type E fractures occurred above 550°F. No fractures of Types B, C, or D were observed for the non-leaded steels. This temperature of 550°F also divides the reduction of area versus test temperature curve into two regions. Below 550°F, the reduction of area remains constant or decreases with increasing temperature. Above 550°F, the reduction of area rapidly increases. Therefore, Type A fractures correspond to the part of the reduction of area versus test temperature curves where the ductility change is small, while Type E fractures lie on the portion of the curves where the ductility is increased appreciably.

Similarly, a number of conclusions can be reached regarding the fracture behavior of the leaded steel from examining Table 1 and Figure 14. Each fracture type tended to occur within a specific temperature range regardless of strength level:

Type A	Room temperature to 400°F
Type B	400°F to 600°F (onset of embrittlement)
Type C	600°F to 650°F (severe embrittlement)
Type D	650°F to 900°F (maximum embrittlement)
Type E	Above 900°F.

Type C fractures were relatively rare and were not observed in the L-18, L-22, and L-24 series. A possible explanation of this observation may be that no specimens were tested in the narrow temperature range where this type of fracture prevailed. This explanation is in keeping with the observation that the temperature range for Type C is only from 600°F to 650°F.

6.2.2. MICROSCOPIC ANALYSIS USING THE ELECTRON MICROSCOPE

6.2.2.1 HIGH STRENGTH LEADED MATERIAL. Since fractures A and E are not associated with the embrittlement, it was decided to examine these first with the electron microscope. A Type A fracture was previously defined as a low temperature cup and cone fracture consisting of a fibrous central region, a radial shear intermediate region, and a shear lip outer region. Replicas were made from each of these regions for L-24 material fractured at room temperature. Figures 15, 16, and 17 are fractographs taken from the fibrous, radial shear, and shear lip regions, respectively, for this high strength leaded material. The fracographs show that transgranular fracture by microvoid coalescence ("dimpled rupture") typifies all three regions. There is no basic difference between the fracture surfaces of the fibrous and radial shear zones, but the dimples on the shear lip are more elongated than those in the other two regions. As previously mentioned, it is generally known that a shear area is characterized by "elongated dimples." Therefore, additional fractographs representative of shear areas for Type B, C, D, and E fractures will not be included in this report.

A Type E fracture was previously defined as a high temperature cup and cone fracture consisting of a fibrous center region and shear lip outer region. Fractographs of the fibrous center region taken from high strength L-20 material tested at 900°F are shown in Figures 18a and 18b. Due to the fact that these fractures occurred at high temperatures, the surfaces were badly oxidized. The surfaces appear to have been formed by a dimpled rupture process and the fractographs may be said to show "oxidized dimples." Whether the dimples present are in an oxidized form or not does not change the conclusion that Type E fractures took place in a ductile transgranular mode.

Type B fracture is characterized by a very rough surface with a very small shear lip. Replicas were made from L-24 material tested at 550°F. Typical fractographs taken from the very rough surface are shown in Figures 19a, 19b, 20a, and 20b. These fractographs show an intimate mixture of intergranular and transgranular models of failure, and indicate that in virtually all cases an inclusion, labled I on the photographs, was present in each region of intergranular grain facets. The area immediately surrounding the inclusion was intergranular, but the area surrounding the intergranular region was transgranular. This seems to suggest that some kind of radial crack growth originating at the inclusion took place in this fracture type.

A fracture of C-Type took place on a 45° plane to the axis of the tensile specimen (shear failure) but there were small flat regions of "fish eyes" located on the fracture surface. Replicas of a region containing several of these small "fish eyes" were taken from L-20 material tested at 600°F. Figures 21a and 21b show a region taken from a cluster of small "fish eyes"; this region shows both an intergranular and transgranular mode of failure for a Type C fracture. As in the Type B fracture, note the inclusion, I, present in the region of grain facets. The area immediately surrounding the inclusion was intergranular, but as the failure progressed radially from the inclusion the mode of failure changed from intergranular to transgranular as is evident from the dimples and "river markings." Thus, though the Type C fracture appearance was very similar to that for Type B, there are two differences between these types. First, the extent of intergranular fracture was greater and the micro-cracks were larger in Type C. Second, at the onset of final fracture the remaining section failed in shear on a 45° plane in Type C and in tension normal to the tensile axis in Type B. Otherwise, the basic fracture process was the same for these two fracture types.

A schematic drawing, Figure 22, is used to show the location of the origin, intermediate region, outer region, and shear lip in a Type D fracture. A preliminary electron microscope examination of a Type D surface taken from L-20 material tested at 800°F gave the following results:

1) The origin, located on the flat "fish eye" near the outer surface of the fracture, is completely intergranular as can be seen by the fractographs in Figures 23a and 23b. Note the "rock candy" appearance of the fracture surface.

2) The surrounding intermediate region on the flat "fish eye" is a mixture of both intergranular and transgranular (Figure 24).

3) The outer region of the "fish eye" is almost completely transgranular (Figure 25).

4) The shear lip surrounding the "fish eye" is completely transgranular.

A closer examination near the origin of a Type D fracture revealed that an inclusion was usually present in each region of intergranular grain facets (Figure 26). The inclusion is located adjacent to the letter I on the fractograph.

Previously reported metallographic and electron probe microanalysis studies (see Appendix B) have indicated that the lead forms envelopes around the inclusions in leaded steel. With this information and the evidence provided by the fractographs, a fracture process explaining the maximum loss of ductility associated with a Type D fracture will be proposed in the Discussion Section.

Some quantitative fractography was done on a Type D fracture. Figure 27 shows the percentage of intergranular fracture — usually estimated — as a function of crack length across the "fish eye." From an examination of this curve, it is possible to state that at the origin the fracture was nearly 100 per cent intergranular. As the crack propagated, the fracture mode changed from intergranular to transgranular. When the crack reached the outer region of the "fish eye," the fracture mode was almost 100 per cent transgranular with a "dimpled rupture." The purpose of constructing this curve was not to show accurate values of the percentage of intergranular fracture but rather to establish the fact that the percentage of intergranular fracture decreased as the crack propagation took place.

6.2.2.2 LOW STRENGTH LEADED MATERIAL. Examination of Type A and E fractures for the lower strength leaded specimens showed that only ductile transgranular failure existed on the fracture surface. The fibrous central region, radial shear intermediate region, and shear lip outer region for Type A fractures were characterized by a "dimpled rupture" appearance. Similarly, the Type E fracture surface was of the "oxidized dimpled rupture" type.

Fractographs taken from low strength (120 ksi ultimate) materials which had been classified Type B and C fractures are shown in Figures 28 and 29 respectively. The fractographs show that again the fracture mode was both intergranular and transgranular. However, the outline of the grains in the intergranular portion of these fractographs were not as clear as the grain outline shown in the fractographs for the higher strength leaded material.

A low strength Type D fracture surface (140 ksi ultimate material tested at 700°F was also examined. The results obtained were almost the same as those previously found for the high strength material. The only difference occurred in the intergranular regions of the low strength material (Figure 30) where the outline of the grains had a "crusty" appearance. This appearance may be simply a characteristic of the lower strength material, or it may be due to some oxidation on the fracture surface.

6.2.2.3 HIGH AND LOW STRENGTH NON-LEADED MATERIAL.

Fractographs taken from Type A and Type E fractures of non-leaded materials also reveal that transgranular fracture by "dimpled rupture" characterizes the fracture surface. Examination of the fractographs indicates that both Type A and Type E fractures are very ductile as shown by their "dimpled rupture" appearance; this observation correlates with the large values of reduction of area obtained on the macroscopic level. Thus, from the preceding fractographic analysis of fracture Types A and E, it can be concluded that 4145 steel normally fractures in a ductile transgranular manner.

Section 7

DISCUSSION

Mostovoy and Breyer hypothesized that the embrittlement in the leaded 4145 steel occurring below the melting point of lead can be explained by a vapor transport mechanism.[1] Lead vaporized at a small microcrack adjacent to either the solid or liquid lead envelope around inclusions can be deposited by vapor transport to the root of the crack. This in turn causes further crack propagation. The remaining lead, finely dispersed throughout the steel, acts as an embrittling reservoir for the newly forming crack. Furthermore, they suggested that the decrease in ductility with increasing temperature up to and about 200°F beyond the melting point of lead can be attributed to the rising vapor pressure of lead with increasing temperature. To explain the return of ductility at about 900°F, they proposed the following argument. The number of lead atoms covering the root of the crack is a function of another variable, the condensation coefficient. This coefficient is very sensitive to experimental conditions and is thus difficult to measure. A related and much more easily determined variable is the sticking coefficient. The sticking coefficient may be defined as the total mass gained by the surface at the end of a time interval divided by the total mass impinging on that surface during the same time interval. Generally, it is found that as the temperature is increased, the sticking coefficient decreases to very small values. The number of available lead atoms and the ability to "stick" on the surface determines whether conditions for embrittlement are satisfied. This would seem to indicate that at temperatures much below the melting point of lead, the sticking coefficient would have a very high value, but the vapor pressure would be too low to supply sufficient lead

atoms for embrittlement. As the temperature approaches the melting point of lead, a critical temperature, 400°F, is reached where just enough lead atoms are supplied to the crack root to cause some embrittlement. When the temperature is increased beyond this critical temperature, more atoms are transported to the crack tip, and the embrittlement becomes more severe. This explanation accounts for loss in ductility below the melting point of lead.

Using the above argument, Mostovoy and Breyer were able to explain the return of ductility above 900°F. As the temperature is increased, sufficient lead atoms are available at the root of the crack but not enough are able to stick to cause embrittlement. Therefore, another critical temperature, 900°F, is reached where an atom will not remain on the surface long enough to contribute to the embrittlement. At temperatures above this critical temperature, embrittlement will not take place because the sticking coefficient is too low.

The fractographic evidence obtained in the present study enables us to make some evaluations of the above hypothesis. A close examination of fracture Types B, C, and D (i.e., those associated with loss in ductility) revealed that intergranular fracture took place at the origin of the fracture. Even more significant was the fact that an inclusion was found in the region of these intergranular grain facets. Since previous electron microprobe work has shown the lead to be associated with the inclusion (see Appendix B), it is possible to conclude that lead was a contributing factor to the intergranular fracture. Based on the above information, it is possible to propose a fracture process explaining the loss in ductility associated with leaded 4145 steel tested between 400°F and 650°F. At temperatures in this range, as the load increases, intergranular cracks begin to propagate radially from the inclusions and associated lead envelopes. With further increases in the load, the cracks propagate with sufficient speed to outrun the ability of the lead to concentrate at the crack tip and the remaining section fractures by stretching and microvoid coalescence. Thus, the reduced intergranular cracking occurs because the supply of lead is too small and the mobility too low for the intergranular crack to grow very rapidly. The spreading of these intergranular cracks from the lead stringers below the melting point of lead is in keeping with a vapor transport mechanism. The transgranular crack growth is evidenced by the "river markings," the stretched zones, and the dimples radiating from the intergranular regions.

The previous proposal is further verified by examining the color photograph

at 500X of the golden brown "fish eyes" taken from a Type C fracture (Figure 10b). On the golden brown fracture surface there were small white circular irregularities. These irregularities could have been formed by lead inclusions; if this is true, then the photograph would serve as further evidence supporting the proposed fracture process.

Thus, the embrittlement is caused by the formation of many small intergranular microcracks, 0.0001 to 0.001 in. in diameter, around the inclusions and associated lead envelopes. The crack propagates intergranularly as long as the lead vapor is able to be deposited at the root of the crack. When the crack "outruns" the lead vapor being deposited at its tip, the fracture mode changes from intergranular to transgranular. Thus, the ability of the lead vapor to "keep up" with the propagating crack determines the degree of embrittlement.

Above 650°F, the lead in the envelopes becomes molten. Once an intergranular crack begins to form, the liquid lead can flow into the crack and, except for a small gap at the crack tip, be readily available for embrittlement. Furthermore, the growing crack will continually interact fresh reservoirs of liquid lead. Thus, the origin of the fractures in the range 650°F to 900°F (Type D) would be expected to be completely intergranular. As the crack accelerates it begins to "outrun" the lead and a mixed fracture mode results because more fresh lead reservoirs will still be cut by the propagating transgranular crack. Each time such a lead region is traversed, the mode changes to intergranular. As the crack grows and continues to accelerate the lead has less influence on the mode of failure (Figure 24). This hypothesis is in agreement with the theory concerning vapor transport of the lead atoms across the gap between the liquid lead and the propagating crack tip.

From the preceding analysis, a Type A fracture would correspond to the case where the temperature was too low for a sufficient supply of lead atoms to be transported to the tip of the crack. The fractographs taken of this type of fracture support this hypothesis by showing that no embrittlement had occurred because the mode of fracture was a transgranular "dimpled rupture." A Type E fracture would represent the kind of fracture that resulted when the lead atoms would not stick on the root of the crack because of the high temperature. Fractographs also verified the lack of embrittlement by showing that only a ductile "dimpled rupture" mode of failure existed on the fractured surface. Fracture Type B would correspond to

the case where just enough lead atoms would be transported to the crack apex to start embrittling; in fracture Type C more atoms would be transported, and embrittling would be more serious than in Type B. Since part of the fracture surface for both these fracture types failed in an intergranular manner, the embrittlement was microscopically verified. Fracture Type D would represent the fracture appearance that resulted when a maximum number of lead atoms stuck to the root of the crack. This is verified fractographically by the large intergranular regions located on the fractured surface.

BIBLIOGRAPHY

1. Mostovoy, S. and Breyer, N. "The Effect of Lead on Microcrack Initiation and Propagation in Alloy Steels." Final Report Phase I, Part A: "Embrittlement of Leaded Steels at Intermediate Temperatures," TACOM Technical Report No. 10022 (Final), July 1968.

2. Tiner, N. A. "Fractographic Analysis of AISI 4340 Steel by Optical and Electron Microscopy." Proceedings of the ASTM, 1961, pp 800-808.

3. Hall, C. E. Introduction to Electron Microscopy, McGraw-Hill Book Company, Inc., New York, 1963.

4. Larson, F. and Carr, F. "Tensile Fracture Surface Configurations of a Heat Treated Steel as Affected by Temperature." Transactions of the ASM, Vol. 55, 1962, pp. 599-611.

5. Beachem, C. D. and Pelloux, R. M. N. "Electron Fractography — A Tool for the Study of Micro-mechanisms of Fracturing Processes." Fracture Toughness Testing, ASTM, 1964, pp 210-245.

6. Beachem, C. D. "The Interpretation of Electron Microscope Fractographs." U. S. Naval Research Laboratory Report No. 6360, January 1966.

7. Warke, W. R. "Some Observations on Electron-Microscopic Fractography of Embrittled Steels." Defense Metals Information Center Memorandum 187, Feb. 1964.

8. Phillips, A., Kerlins, V., and Whiteson, B. V. Electron Fractography Handbook, Technical Report ML-TDR-64-416, January 1965.

9. Grube, W. L. and Rouze, S.R. "Preshadowed Replicas for Electron Metallography." Proceedings of the ASTM, Vol. 52, 1952, p. 573.

Table 1. Test Temperatures at Which Each Fracture Type Occurred for Leaded and Non-Leaded Steel Specimens at Various Strength Levels.

Fracture Type	MATERIAL													
	N-12	L-12	N-14	L-14	N-16	L-16	N-18	L-18	N-20	L-20	N-22	L-22	N-24	L-24
A	RT 420°F 530°F	RT	RT 415°F 550°F	RT	RT 400°F	RT	RT 440°F	RT	RT 400°F	RT 386°F	RT 505°F	RT	RT 500°F	RT
B		440°F 545°F		420°F		525°F		480°F 570°F		485°F		550°F		550°F
C		650°F		610°F		650°F				600°F				
D				700°F 800°F		650°F 775°F		680°F 812°F		710°F 800°F 850°F		650°F 780°F 865°F		660°F 745°F
E	690°F 800°F 915°F	775°F 880°F	705°F 850°F	900°F	550°F 675°F 790°F 900°F	880°F	530°F 665°F 807°F 925°F	900°F	600°F 700°F 800°F 900°F	900°F	605°F 790°F		626°F 740°F	

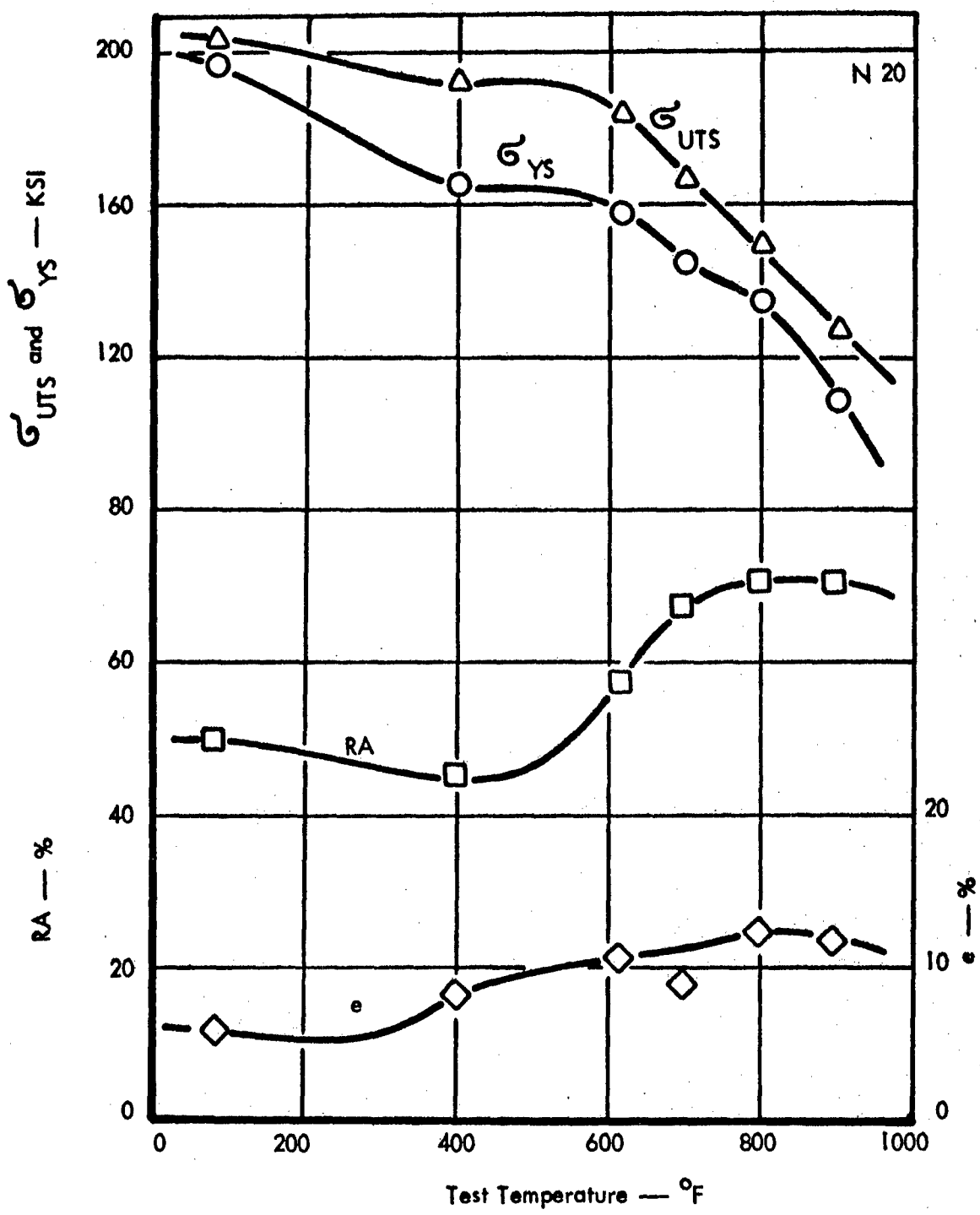

Figure 1. Engineering Tensile Properties of Non-Leaded N20 Material.

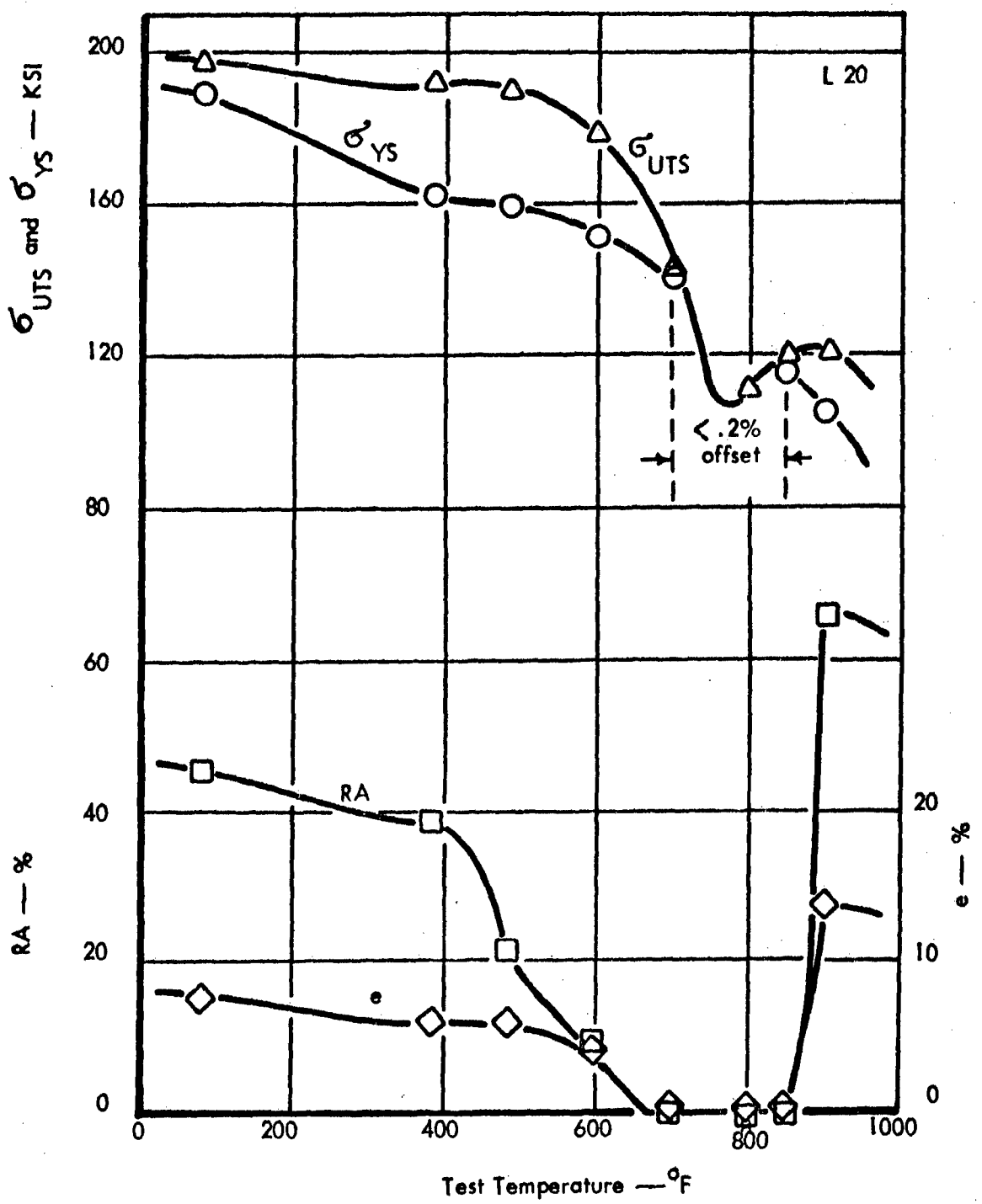

Figure 2. Engineering Tensile Properties of Leaded L20 Material.

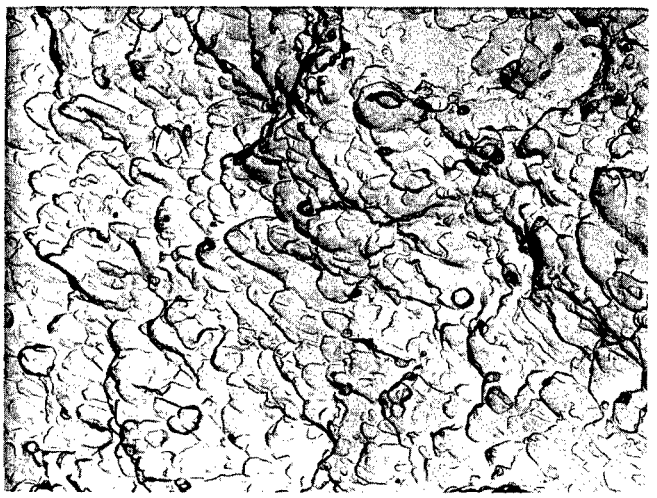

Figure 3. Transgranular Fracture by Microvoid Coalescence ("Dimpled Rupture"). 8,000X

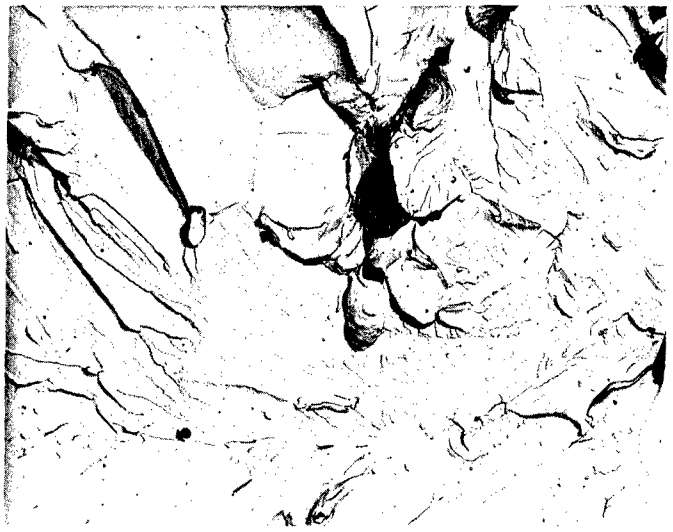

Figure 4. "River Markings" that Characterize Transgranular Fracture by Cleavage. 6,000X

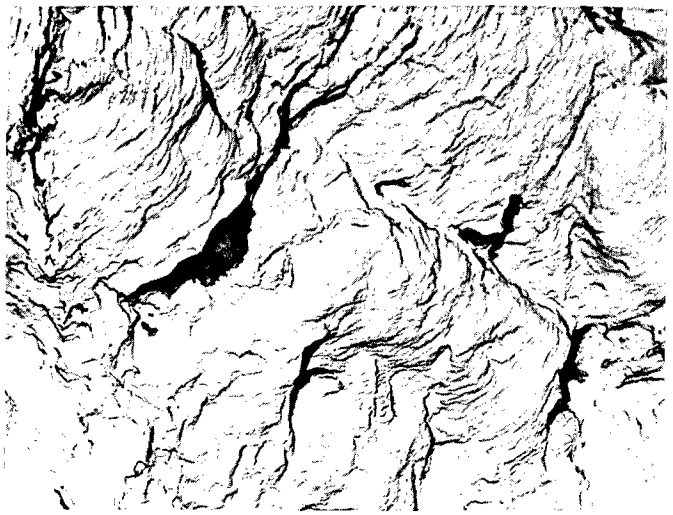

Figure 5. "Striation" that Characterize Transgranular Fracture by Cleavage. 6,000X

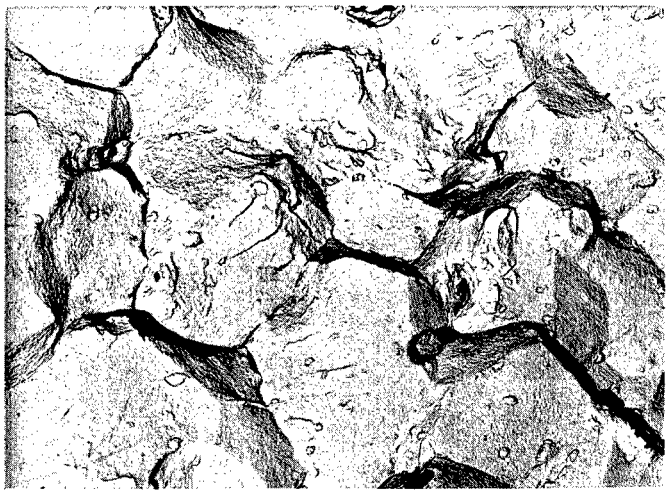

Figure 6. "Rock Candy" Appearance of an Intergranular Fracture Without Microvoid Coalescence. 3,000X

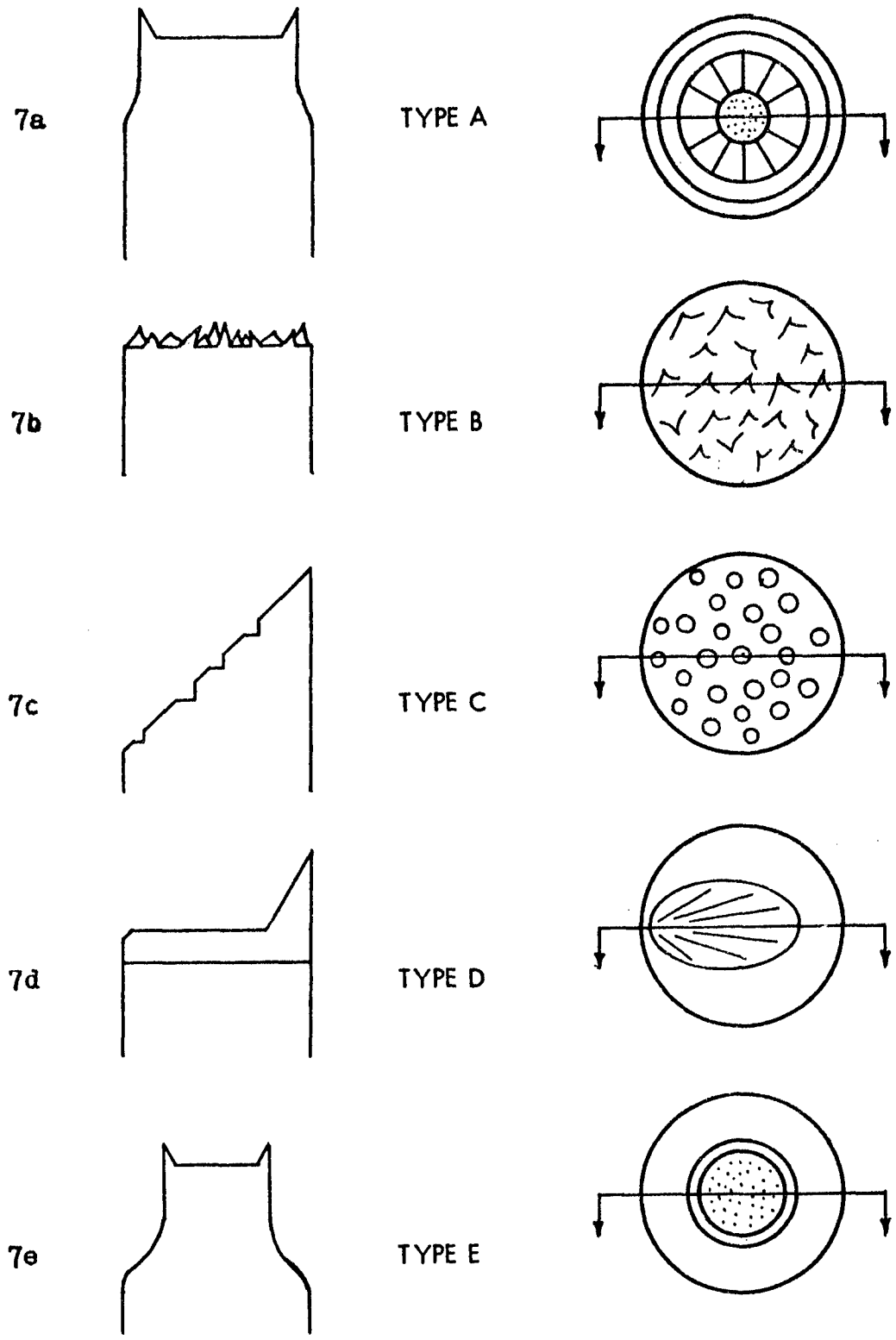

Figure 7. Classification of Longitudinal Tensile Specimen's Fracture Surface.

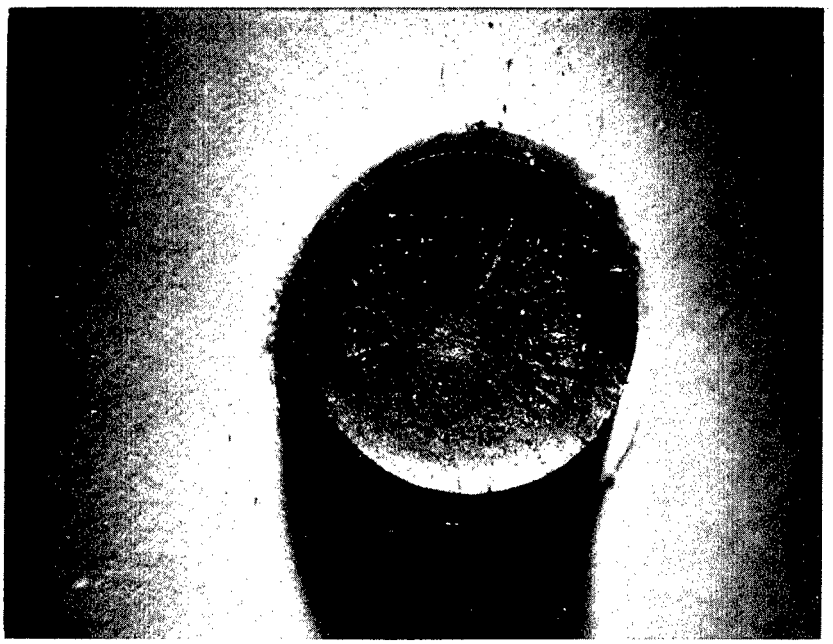

Figure 8. Type A Fracture. Directly Parallel to Axis of Tensile Specimen. 10X

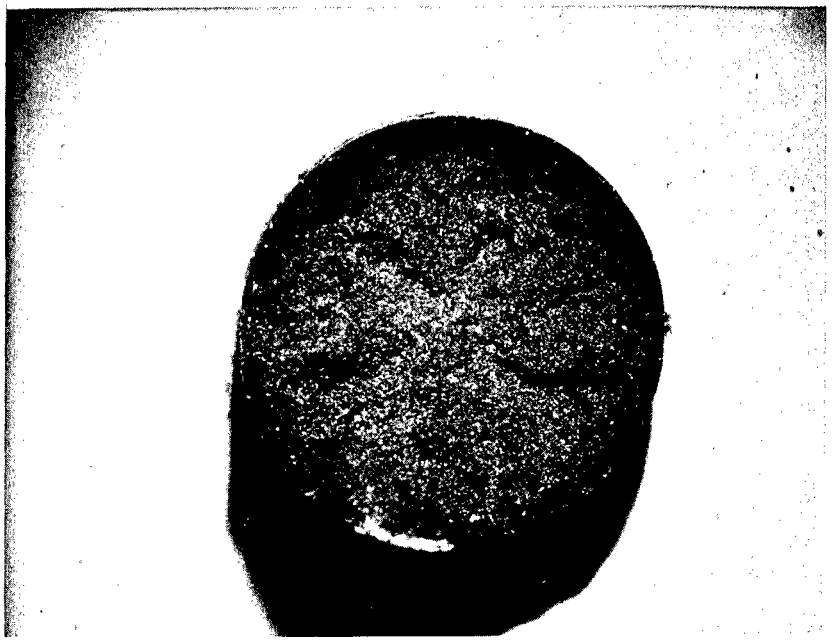

Figure 9. Type B Fracture. Directly Parallel to Axis of Tensile Specimen. 10X

Figure 10a. Type C Fracture. Axis of Tensile Specimen Rotated 45° to Axis of Camera Lens. 10X

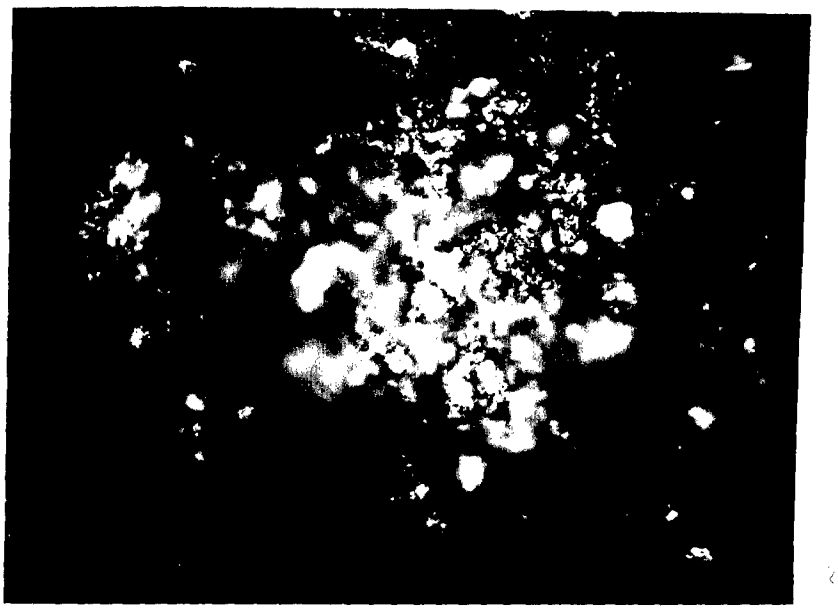

Figure 10b. High Magnification Photograph of the Golden Brown "Fish Eyes" Taken from a Type C Fracture. 500X

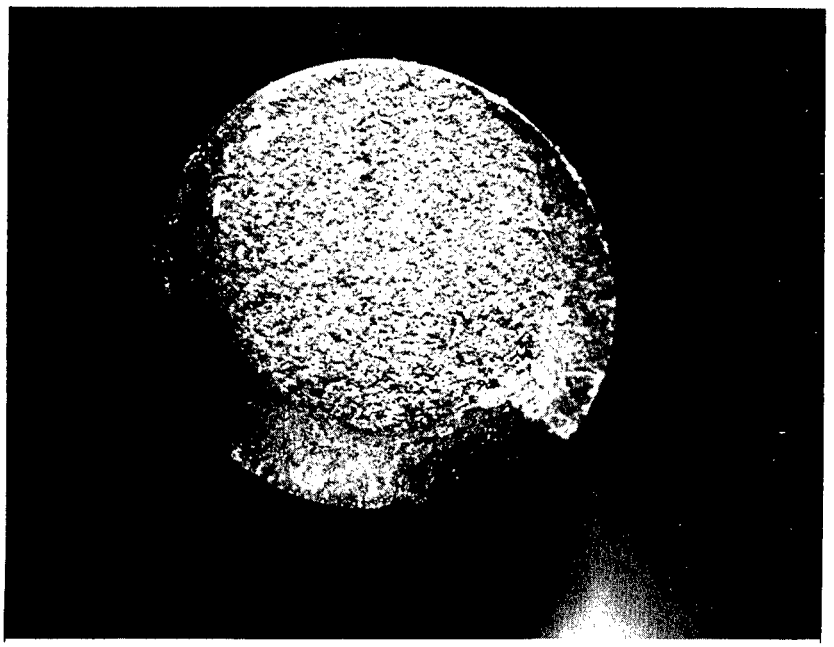

Figure 11. Type D Fracture. Directly Parallel to Axis of Tensile Specimen. 10X

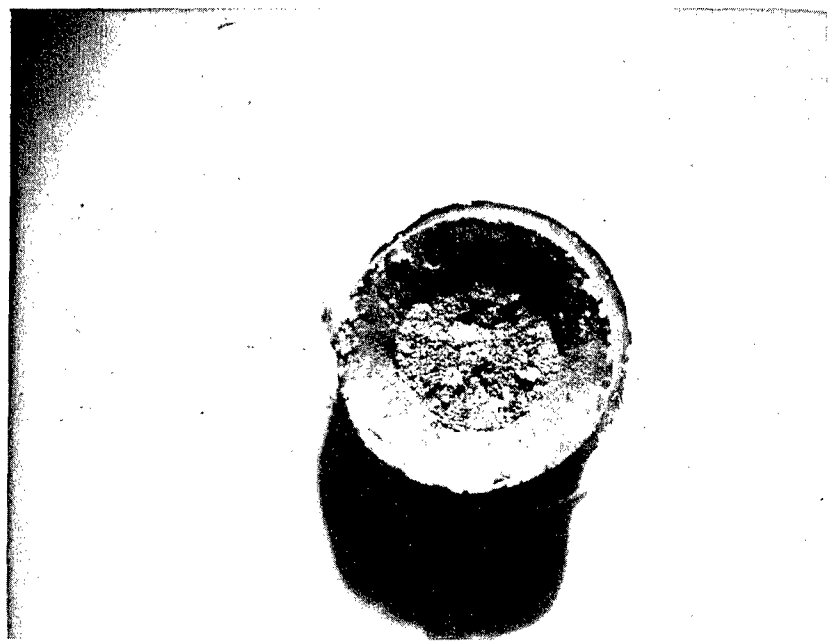

Figure 12. Type E Fracture. Directly Parallel to Axis of Tensile Specimen. 10X

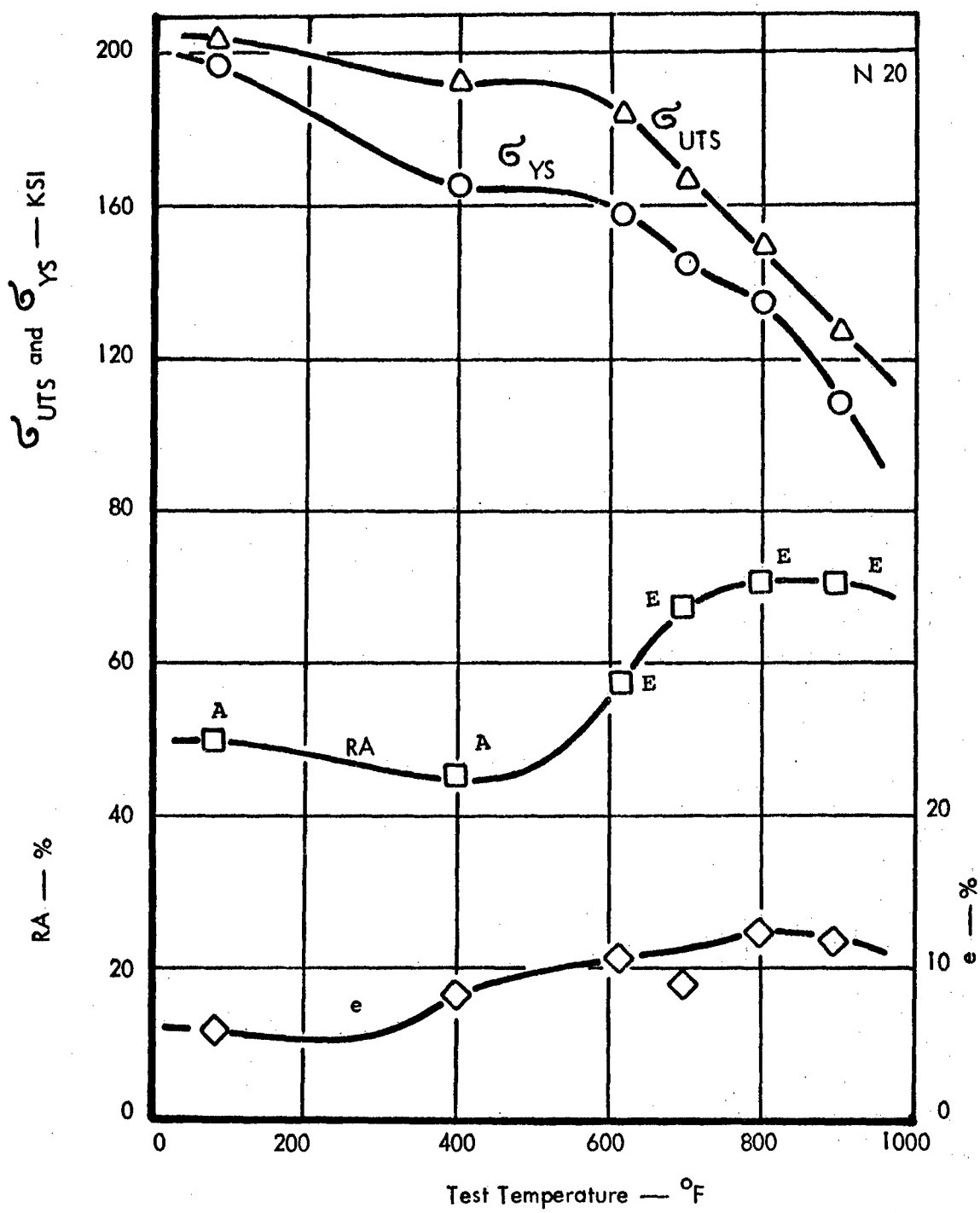

Figure 13. Engineering Tensile Properties of Non-Leaded N-20 Material with Fracture Type Designation Indicated Adjacent to the Corresponding Points on the Reduction of Area Curve.

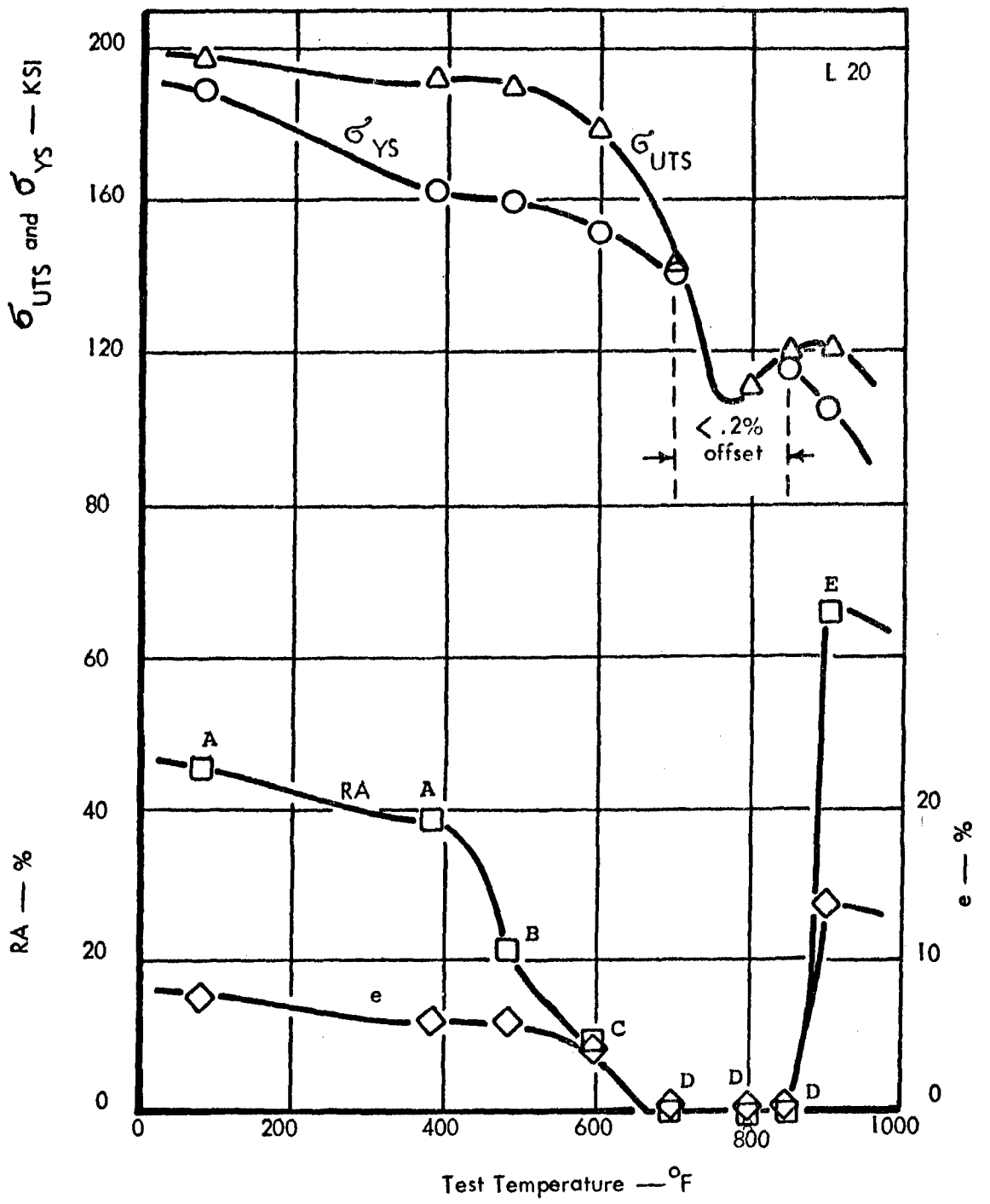

Figure 14. Engineering Tensile Properties of Leaded L-20 Material with the Fracture Type Designation Indicated Adjacent to the Corresponding Points on the Reduction of Area Curve.

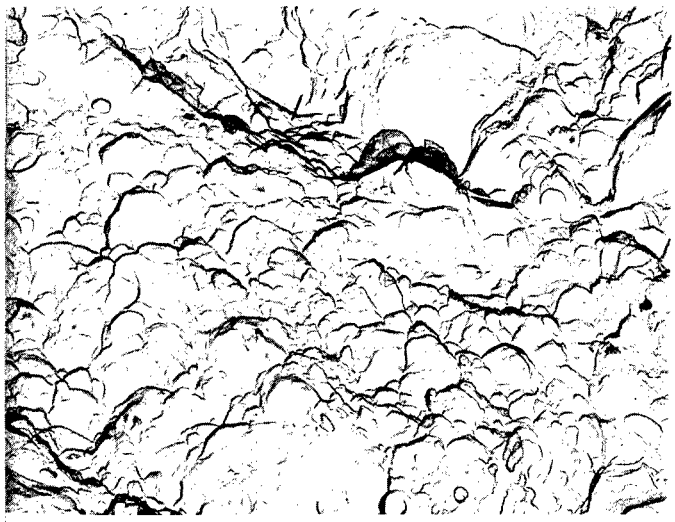

Figure 15. Fibrous Center Region for a Type A Fracture Showing a Complete Transgranular Mode of Failure. 8,000X

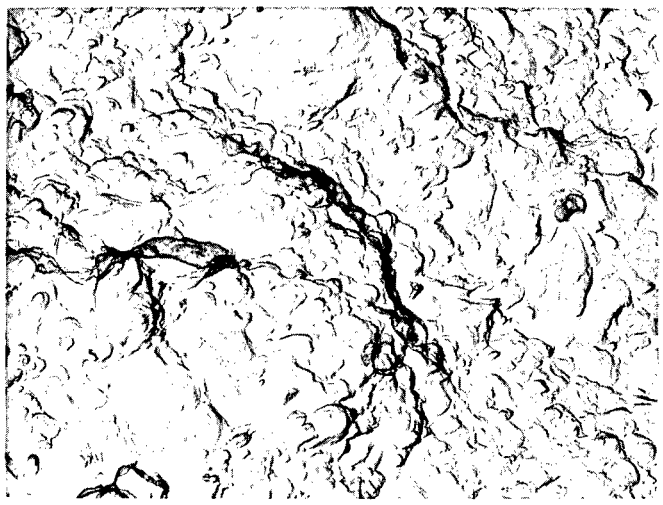

Figure 16. Radial Shear Region for a Type A Fracture Showing a Complete Transgranular Mode of Failure. 8,000X

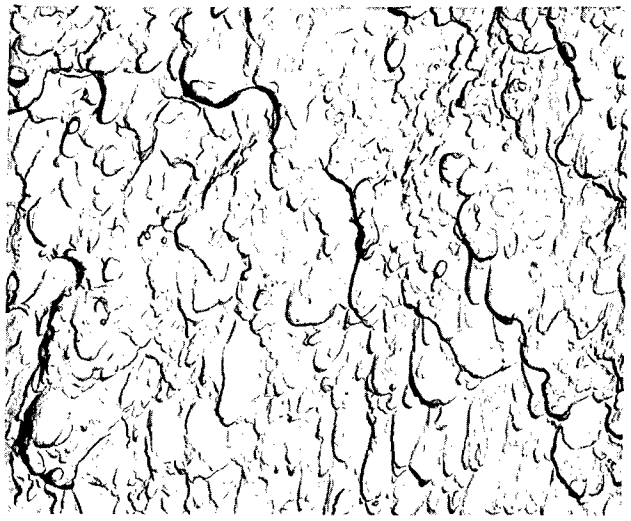

Figure 17. Shear Lip for a Type A Fracture Showing a Complete Transgranular Mode of Failure. 8,000X

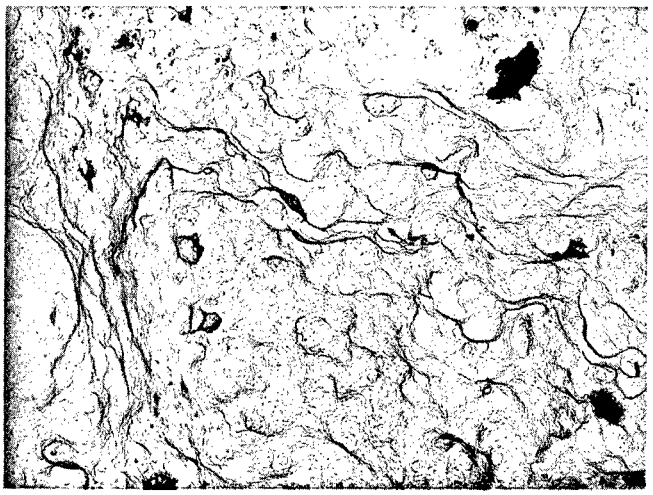

Figure 18a. Transgranular Fracture for a Type E Fracture in the Form of "Oxidized Dimples." 3,000X

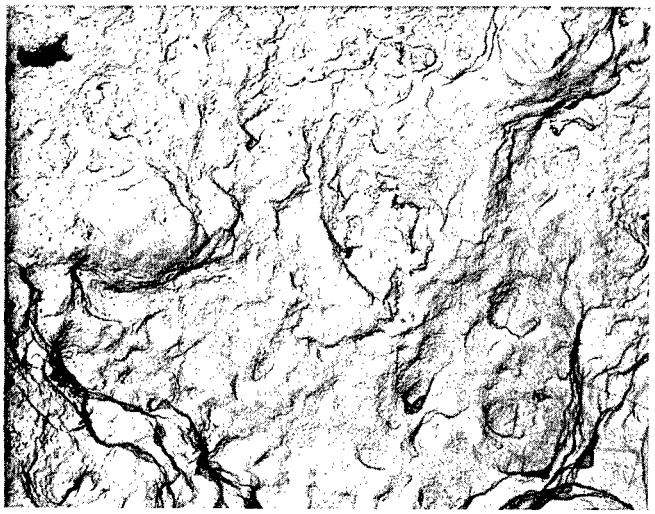

Figure 18b. Transgranular Fracture for a Type E Fracture in the Form of "Oxidized Dimples." 3,000X

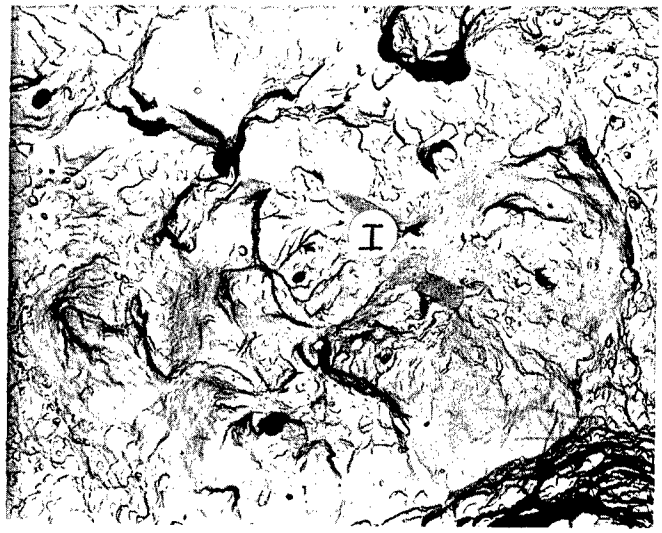

Figure 19a. Primarily Intergranular Fracture for a Type B Fracture. 3,000X

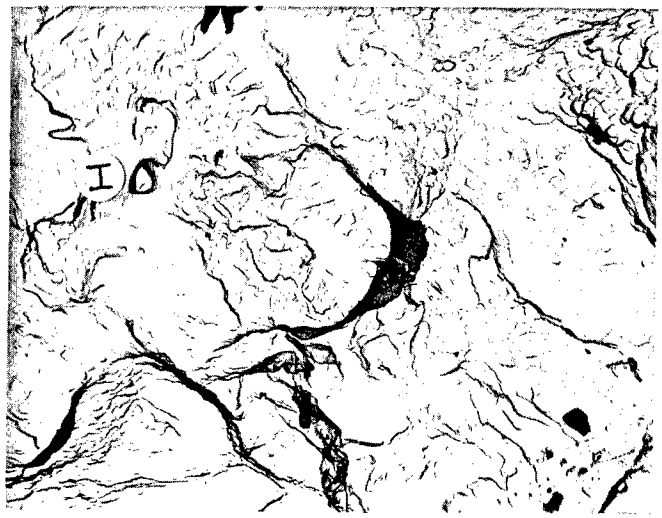

Figure 19b. Primarily Intergranular Fracture for a Type B Fracture. 3,000X

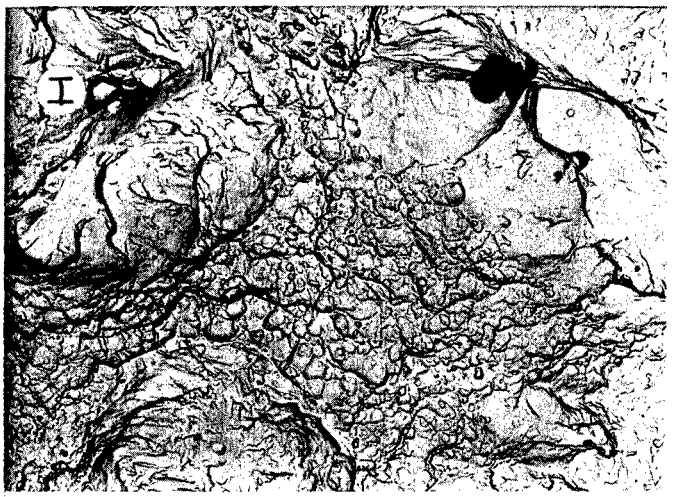

Figure 20a. Region Showing Both an Intergranular and a Transgranular Mode of Failure for a Type B Fracture. 3,000X

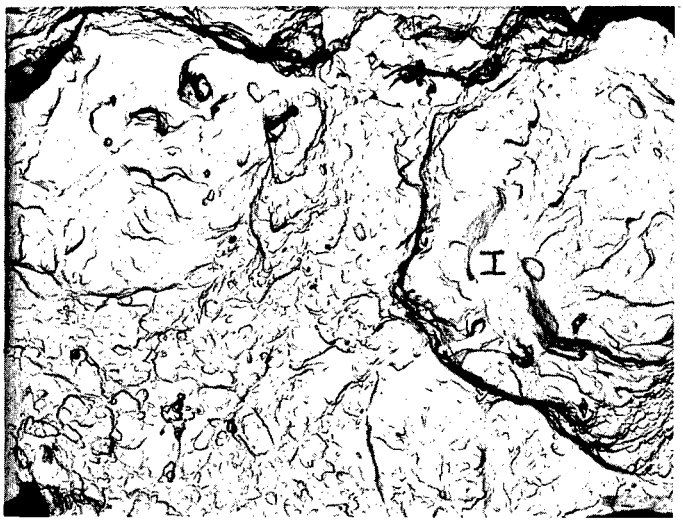

Figure 20b. Region Showing Both an Intergranular and a Transgranular Mode of Failure for a Type B Fracture. 3,000X

Figure 21a. Region Showing Both an Intergranular and a Transgranular Mode of Failure for a Type C Fracture Taken from a Cluster of Small "Fish Eyes." 3,000X

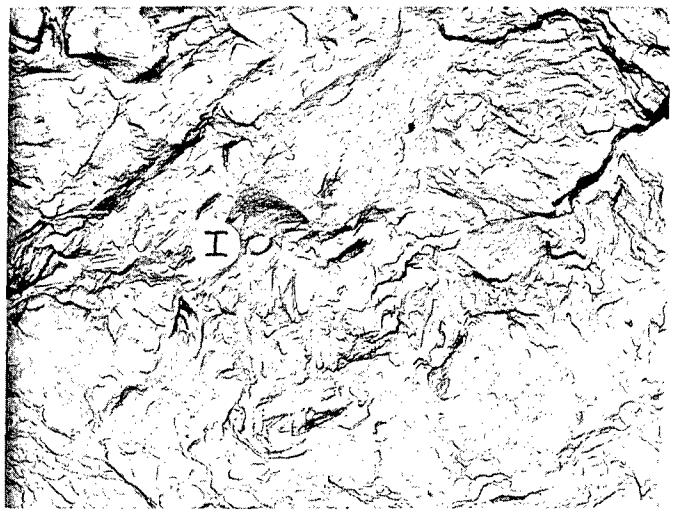

Figure 21b. Region Showing Both an Intergranular and a Transgranular Mode of Failure for a Type C Fracture Taken from a Cluster of Small "Fish Eyes." 3,000X

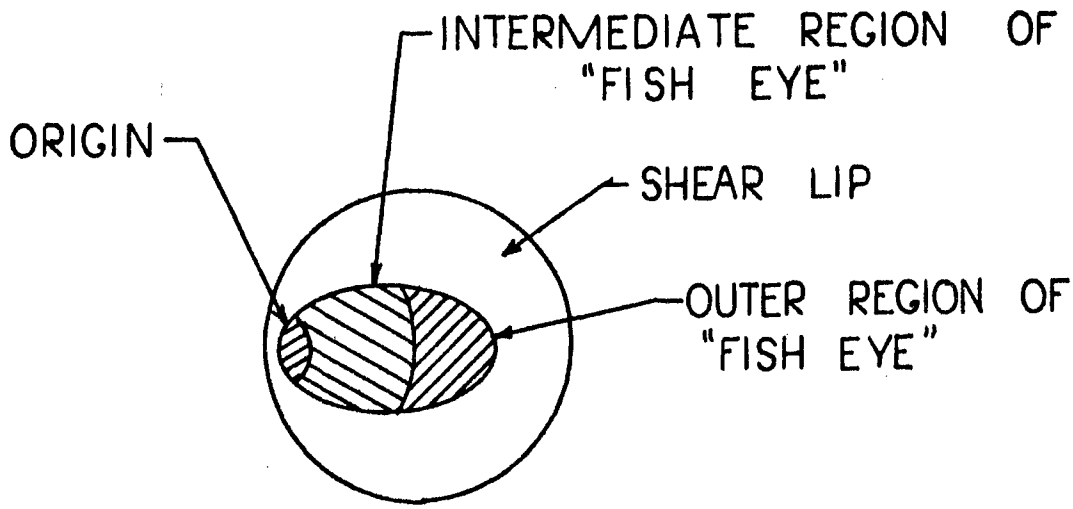

Figure 22. Schematic Drawing of Type D Fracture.

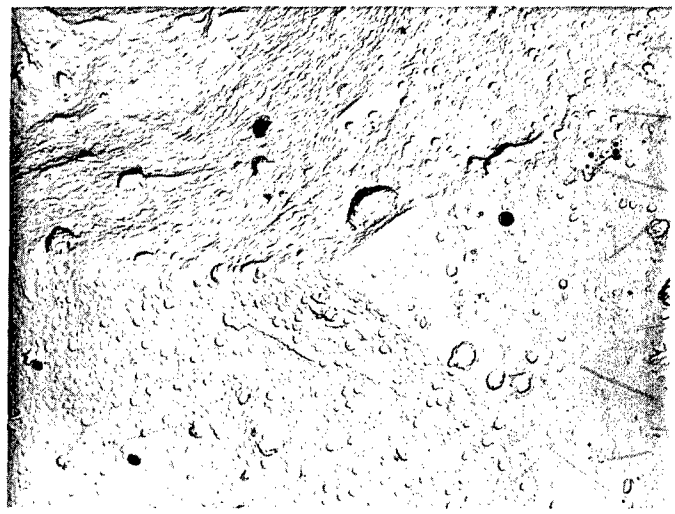

Figure 23a. Origin of Fracture Showing a Complete Intergranular Mode of Failure. 8,000X

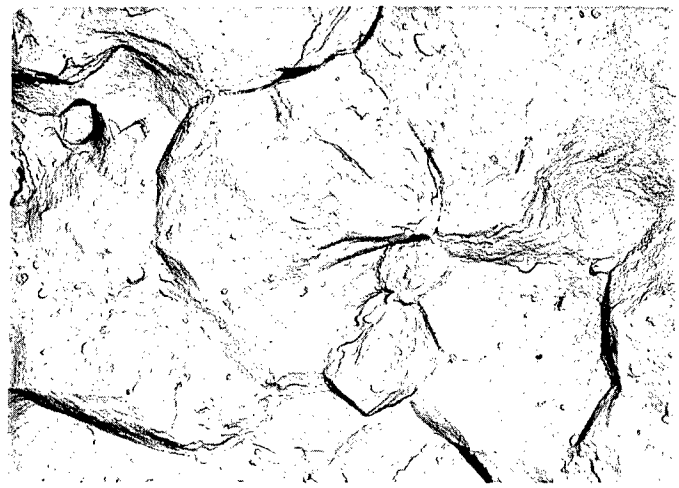

Figure 23b. Origin of Fracture Showing a Complete Intergranular Mode of Failure. 3,000X

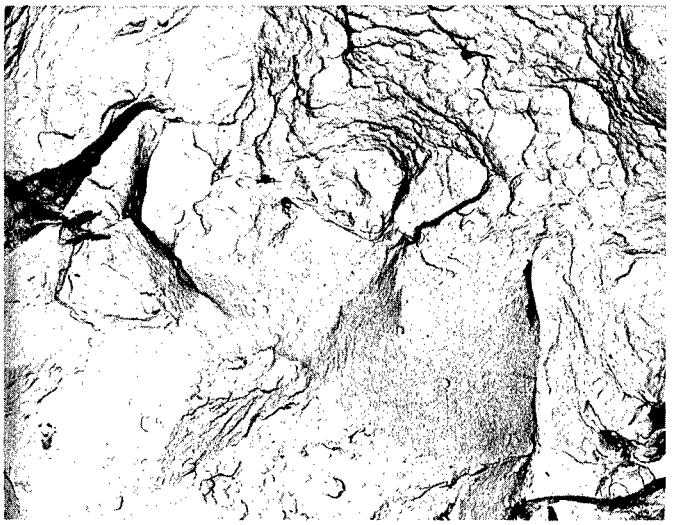

Figure 24. Intergranular and Transgranular Fracture Located in the Intermediate Region. 3,000X

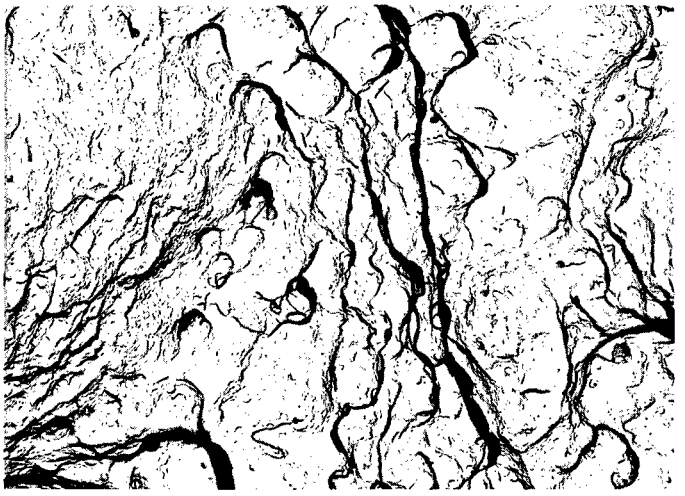

Figure 25. Almost Completely Transgranular Fracture Located in the Outer Region. 8,000X

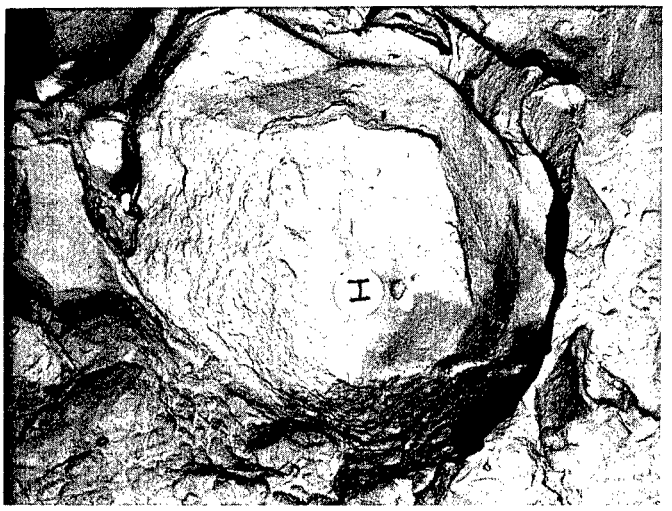

Figure 26. Inclusion Located on Intergranular Grain Facet for a Type D Fracture.

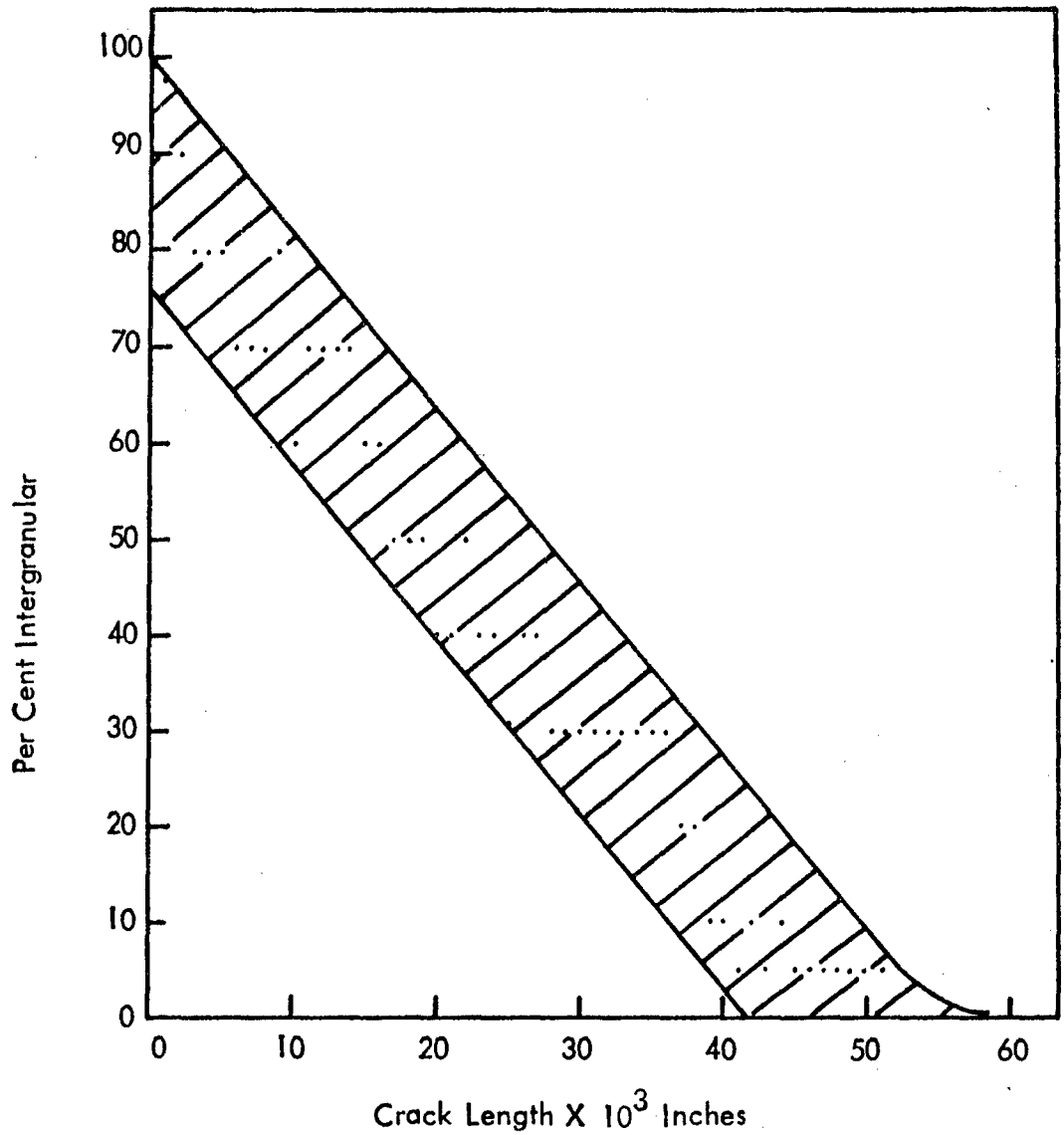

Figure 27. Visual Estimation of Per Cent Intergranular as a Function of Crack Length for a Type D Fracture.

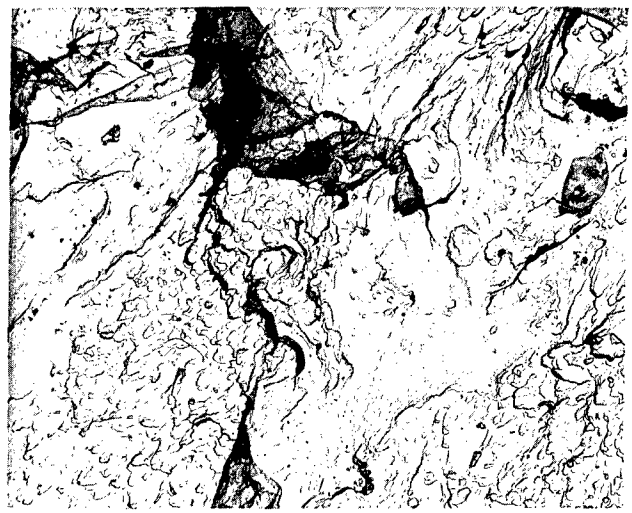

Figure 28. Fractograph of Type B Fracture Taken from a Low Strength Material.

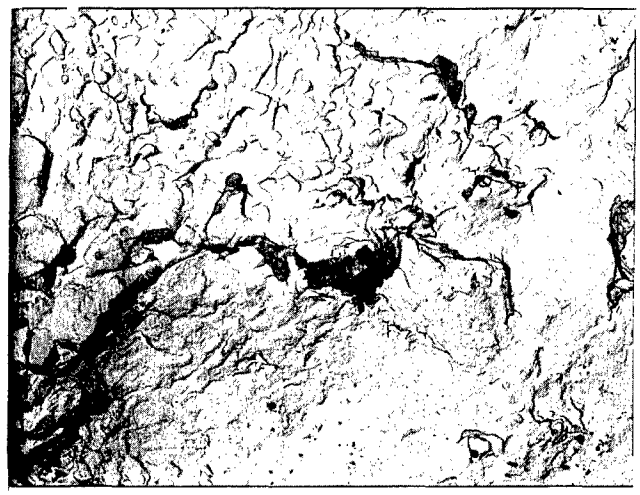

Figure 29. Fractograph of Type C Fracture Taken from a Low Strength Material.

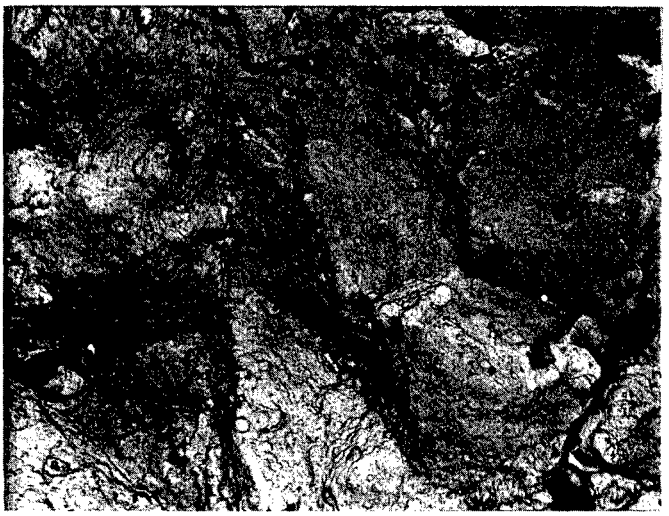

Figure 30. Origin of Low Strength Type D Fracture Showing an Intergranular Mode of Failure.

APPENDIX A

ENGINEERING TENSILE PROPERTY CURVES

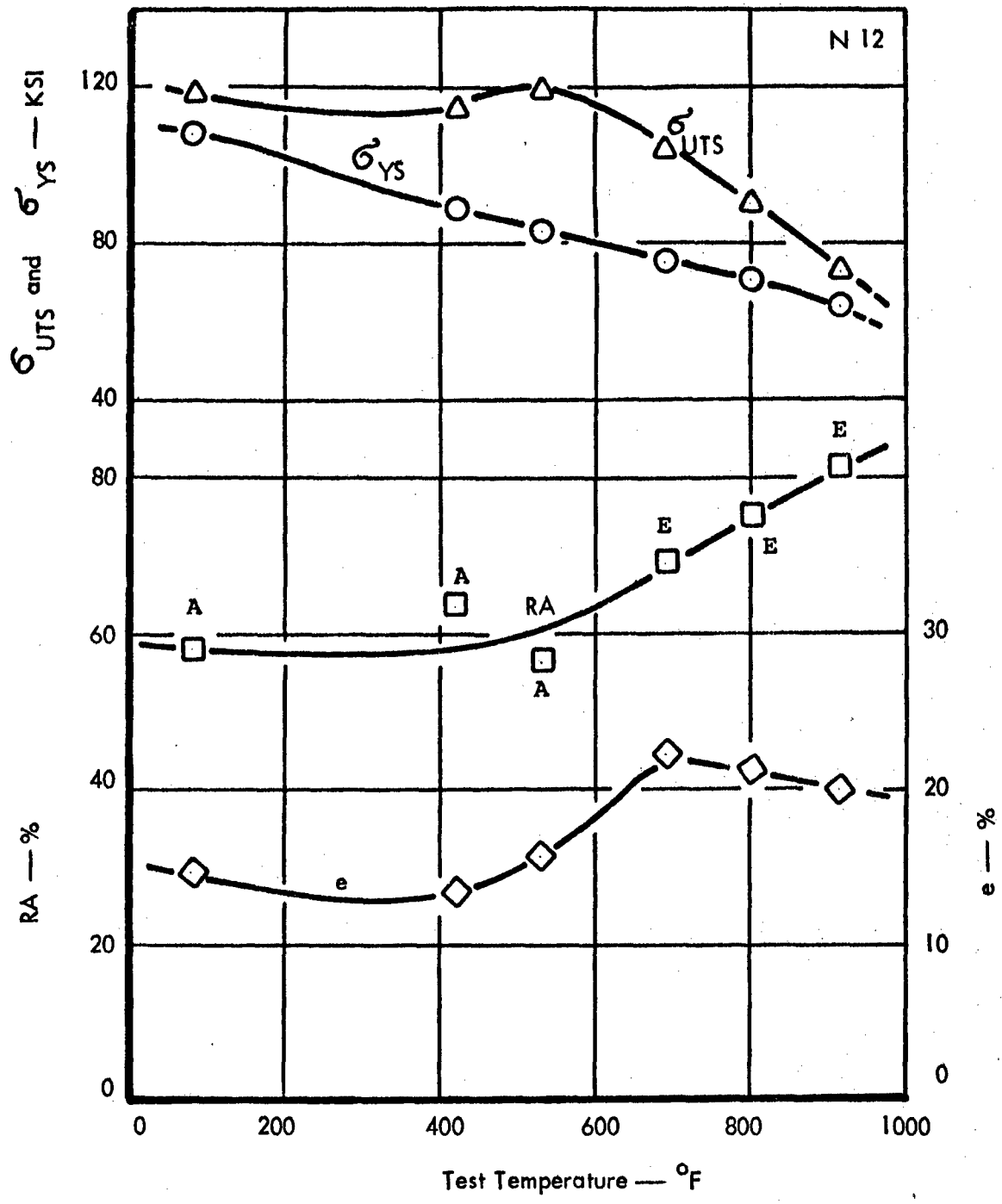

Figure 1A. Engineering Tensile Properties of Non-Leaded N-12 Material.

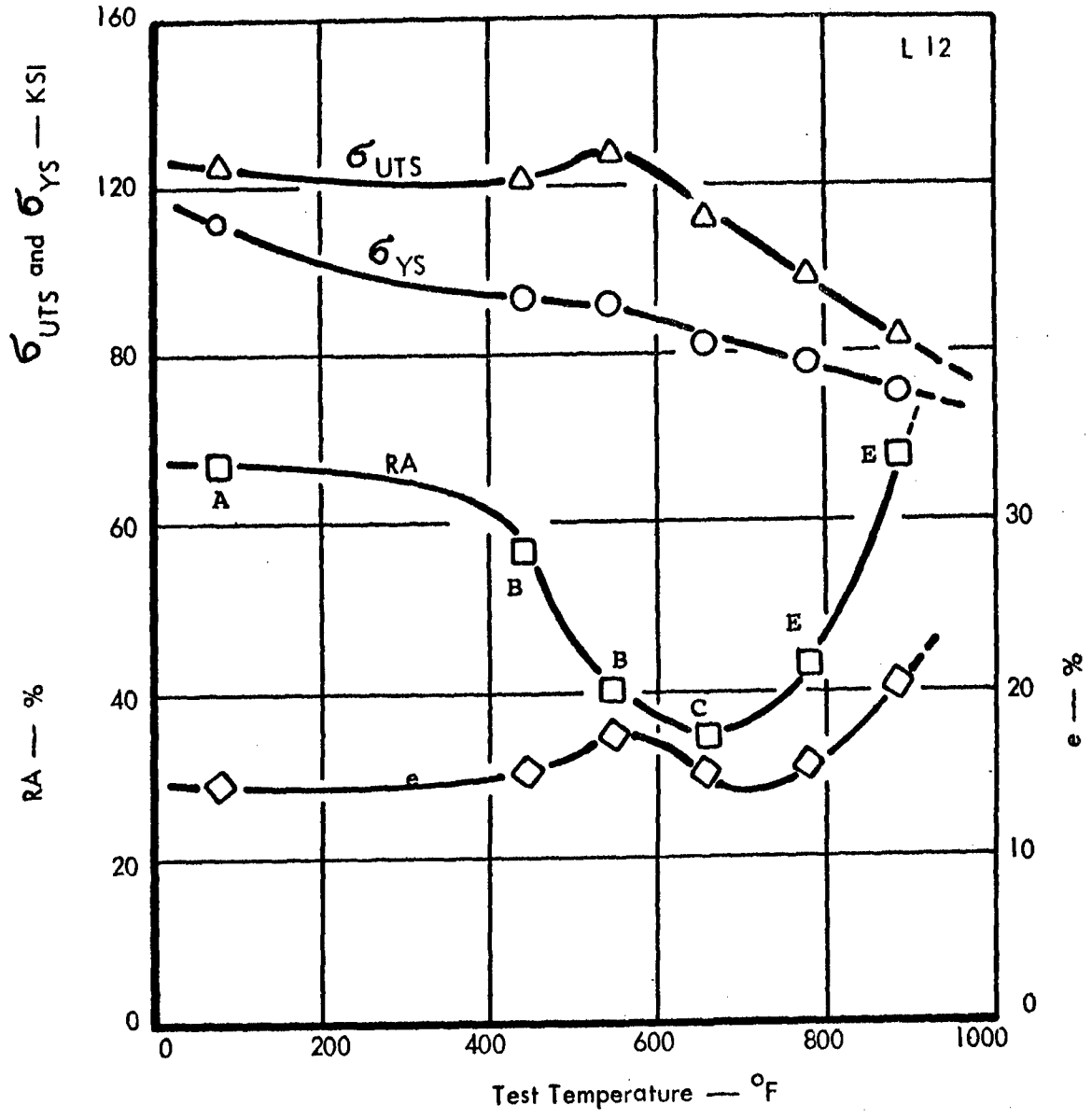

Figure 2A. Engineering Tensile Properties of Leaded L-12 Material.

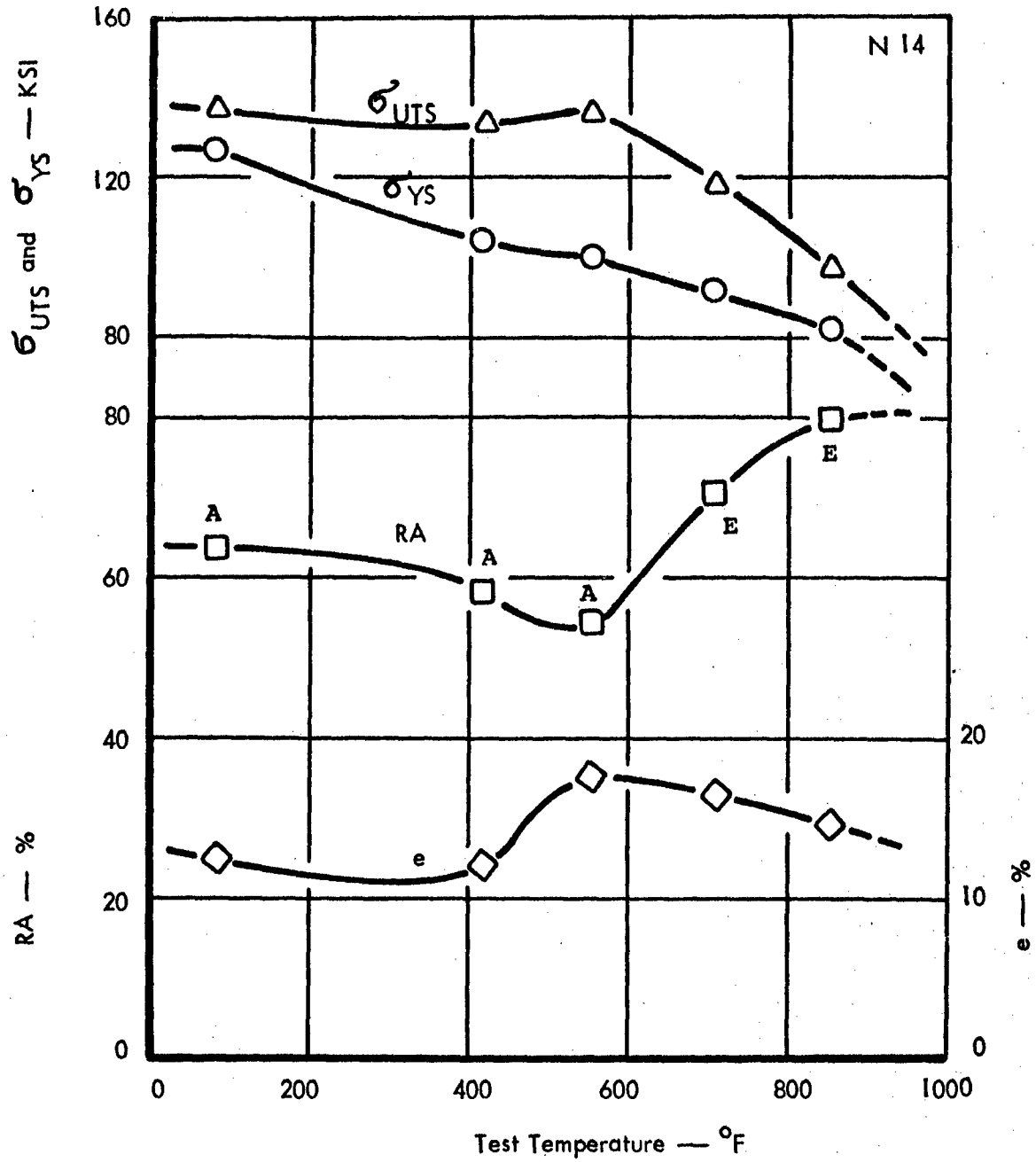

Figure 3A. Engineering Tensile Properties of Non-Leaded N-14 Material.

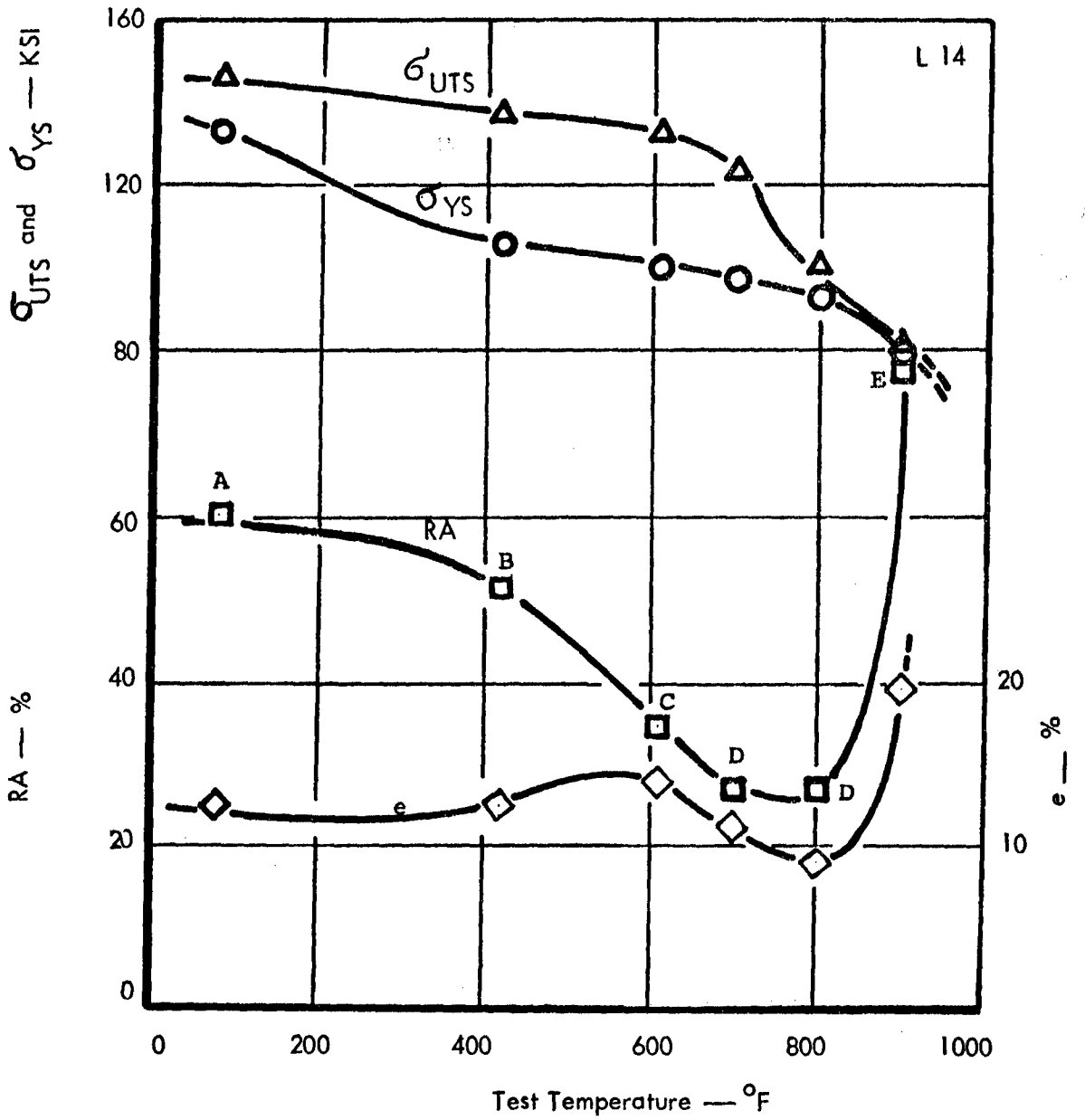

Figure 4A. Engineering Tensile Properties of Leaded L-14 Material.

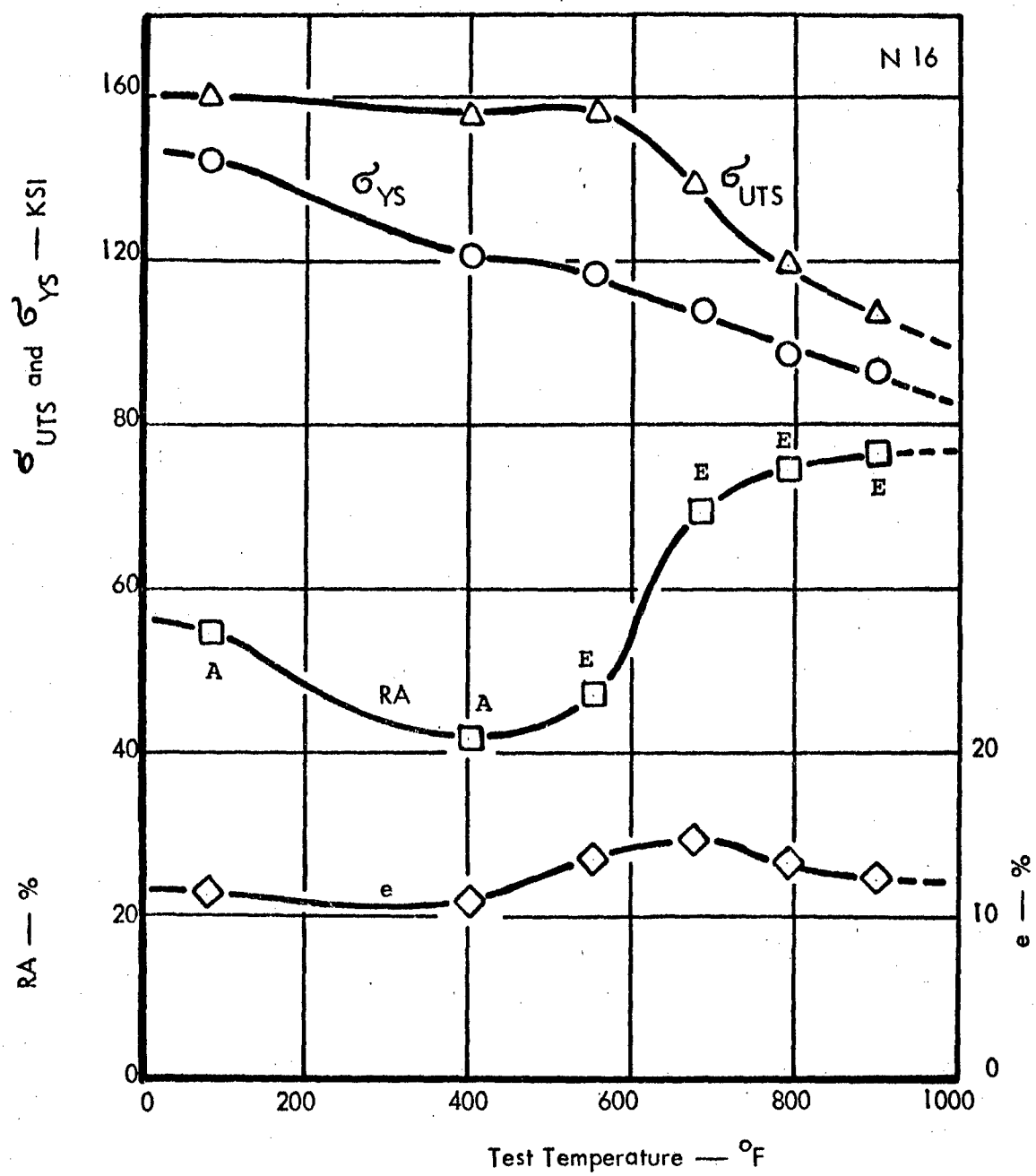

Figure 5A. Engineering Tensile Properties of Non-Leaded N-16 Material.

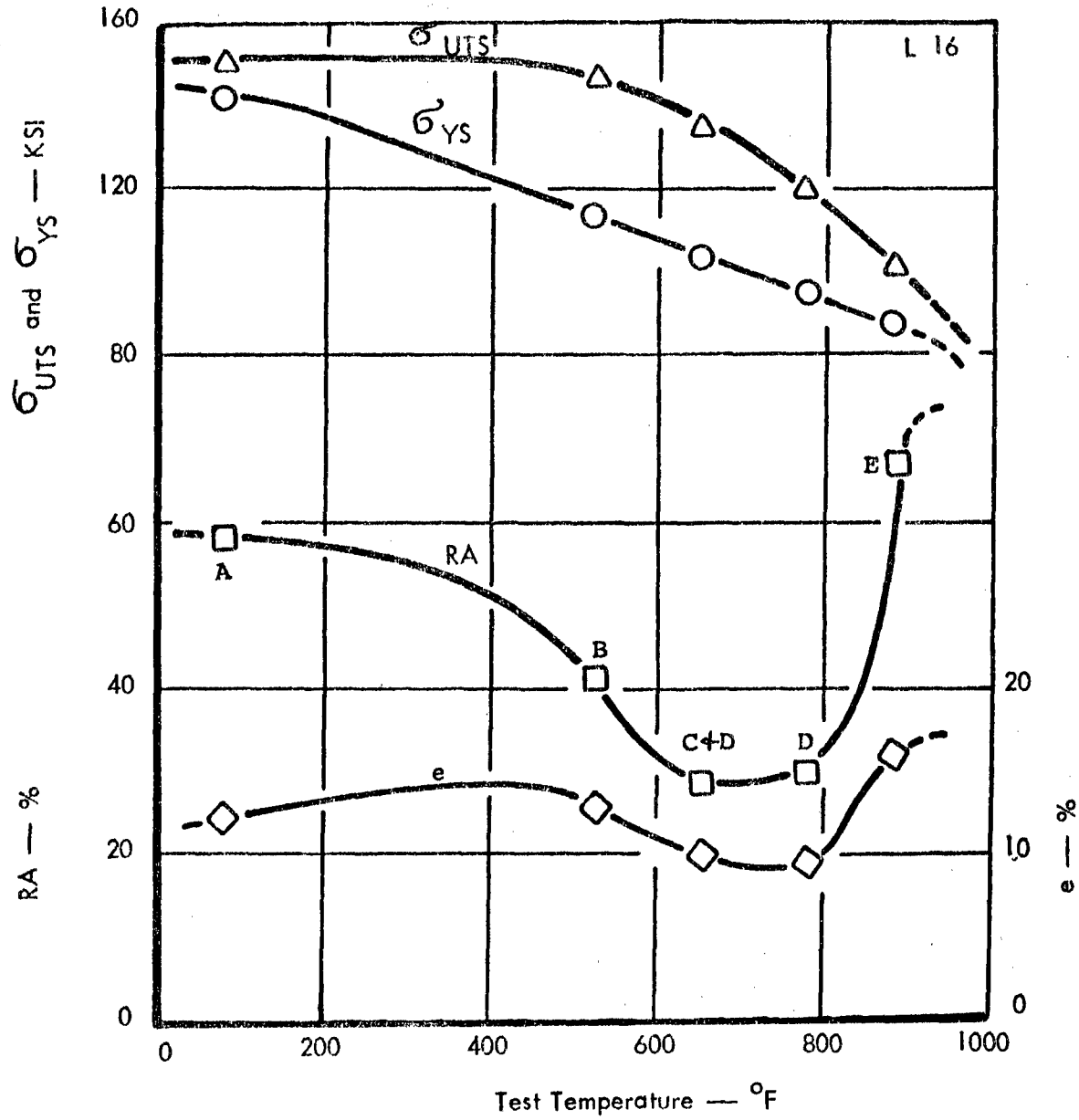

Figure 6A. Engineering Tensile Properties of Leaded L-16 Material.

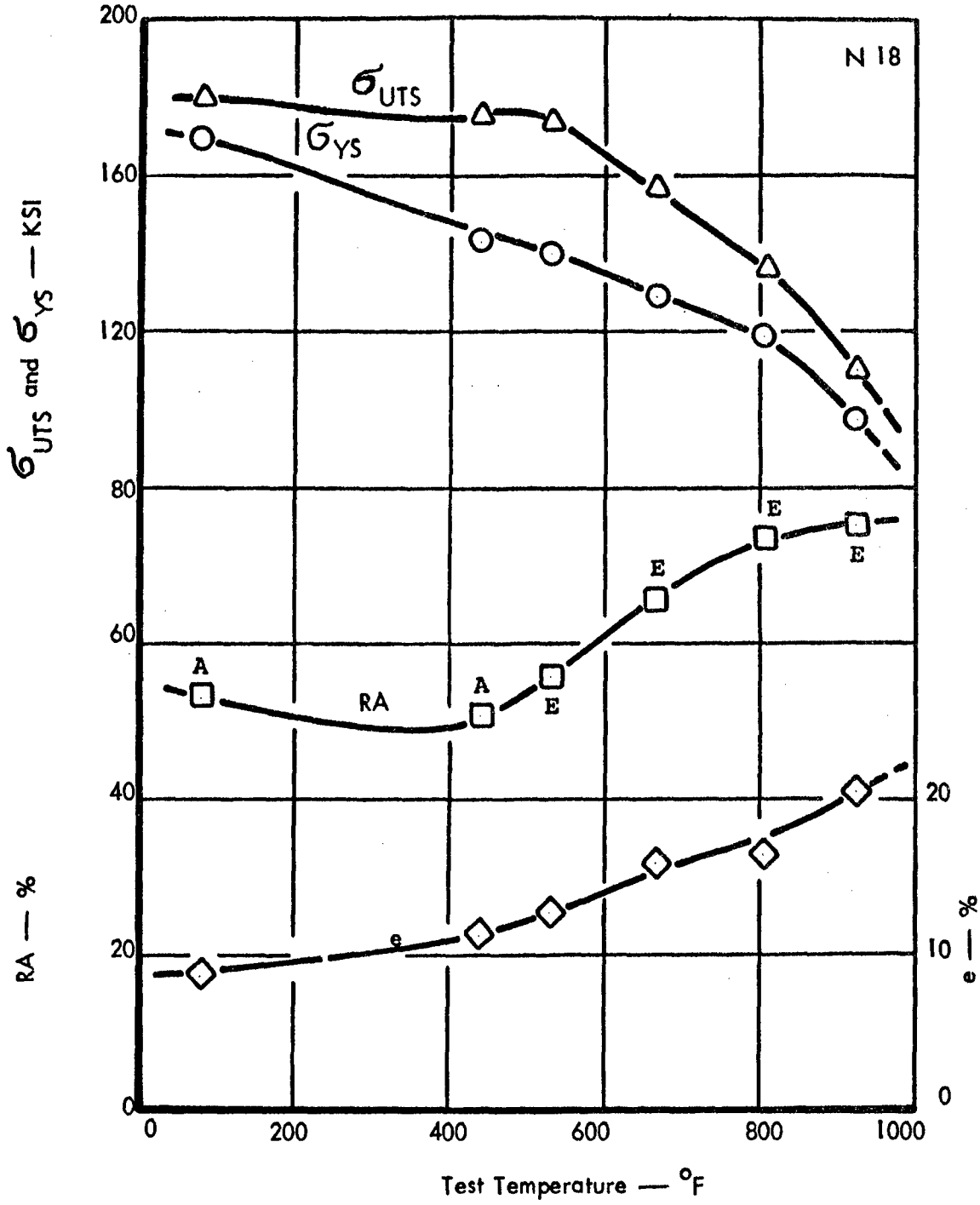

Figure 7A. Engineering Tensile Properties of Non-Leaded N-18 Material.

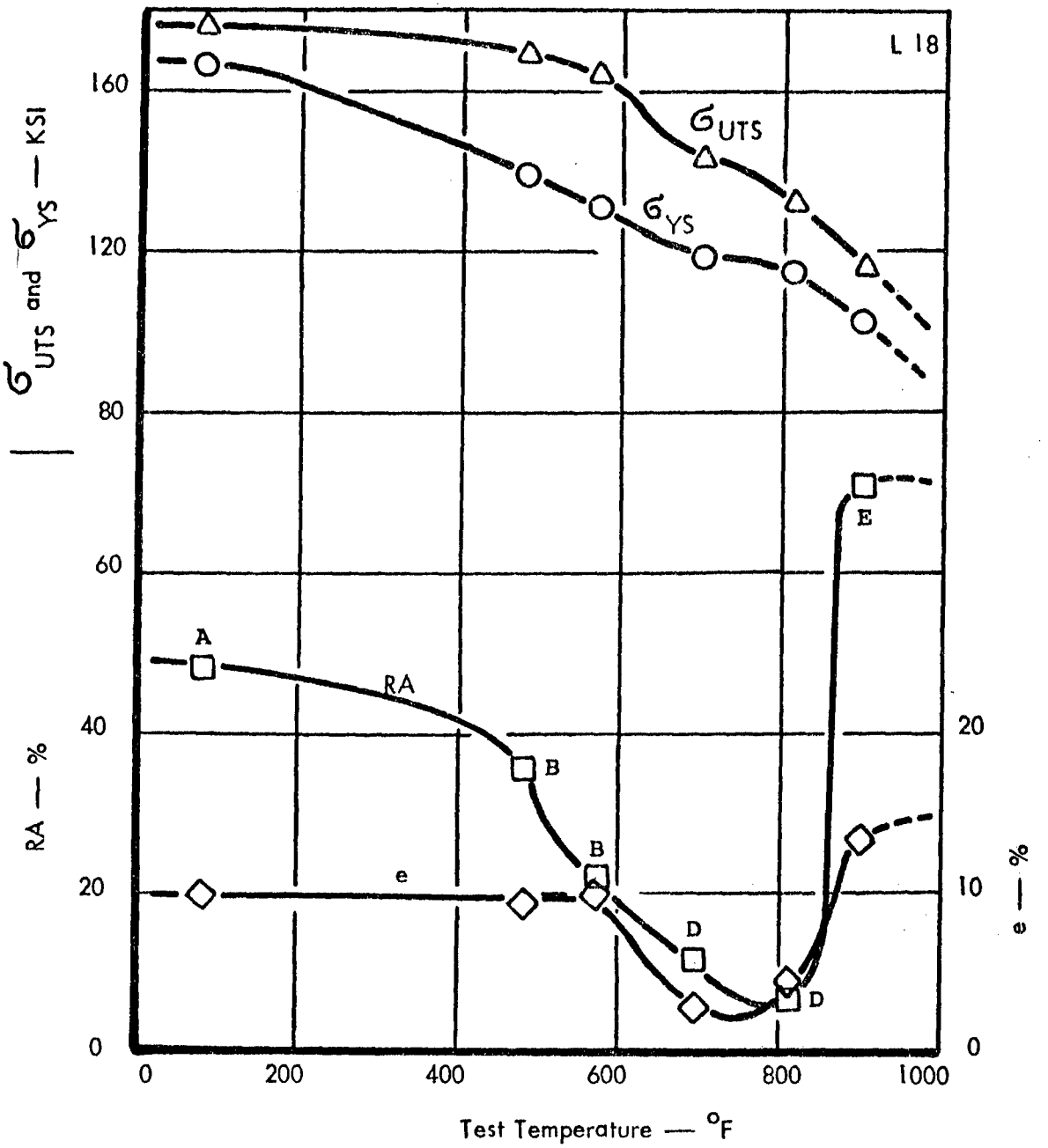

Figure 8A. Engineering Tensile Properties of Leaded L-18 Material.

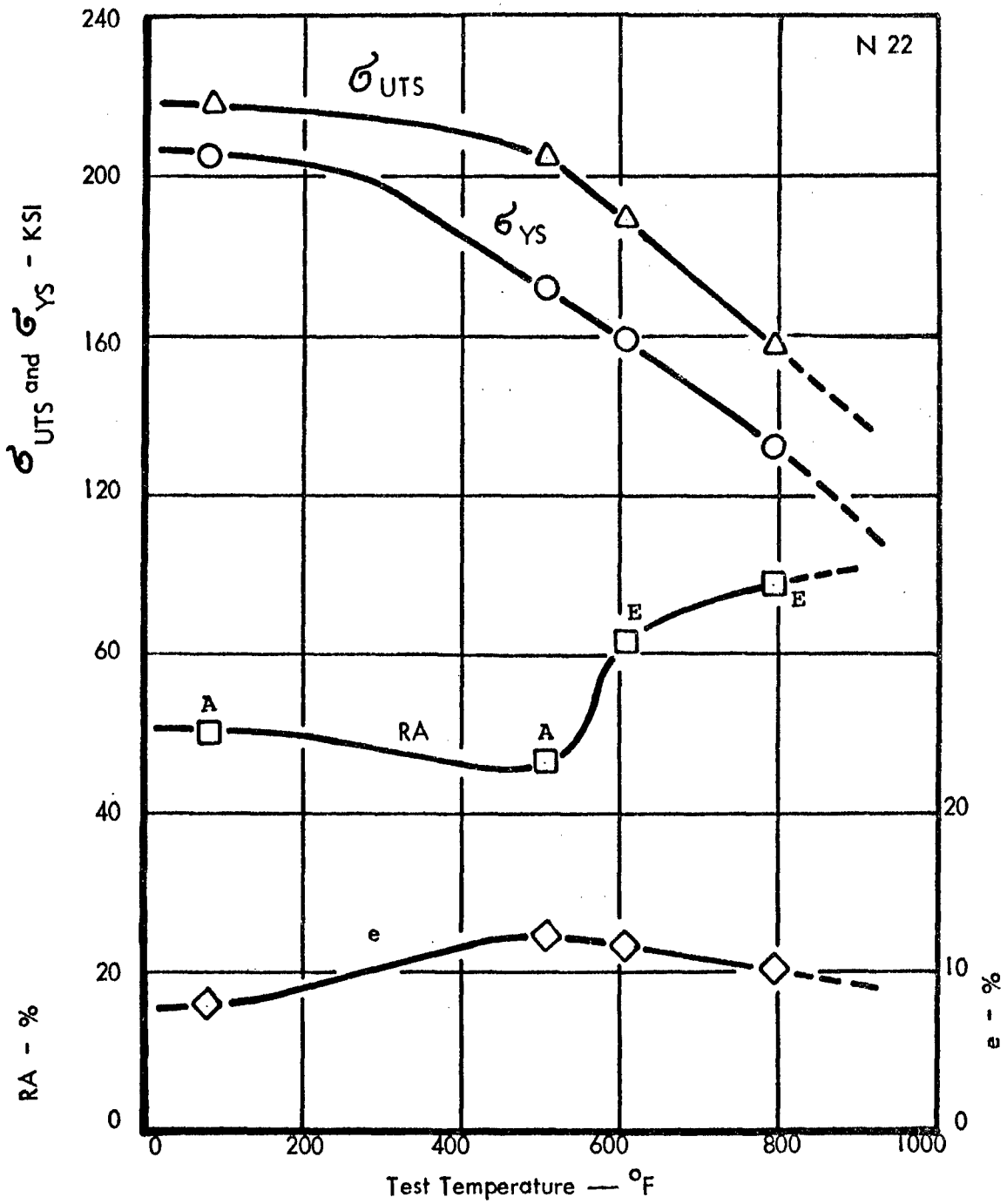

Figure 9A. Engineering Tensile Properties of Non-Leaded N-22 Material.

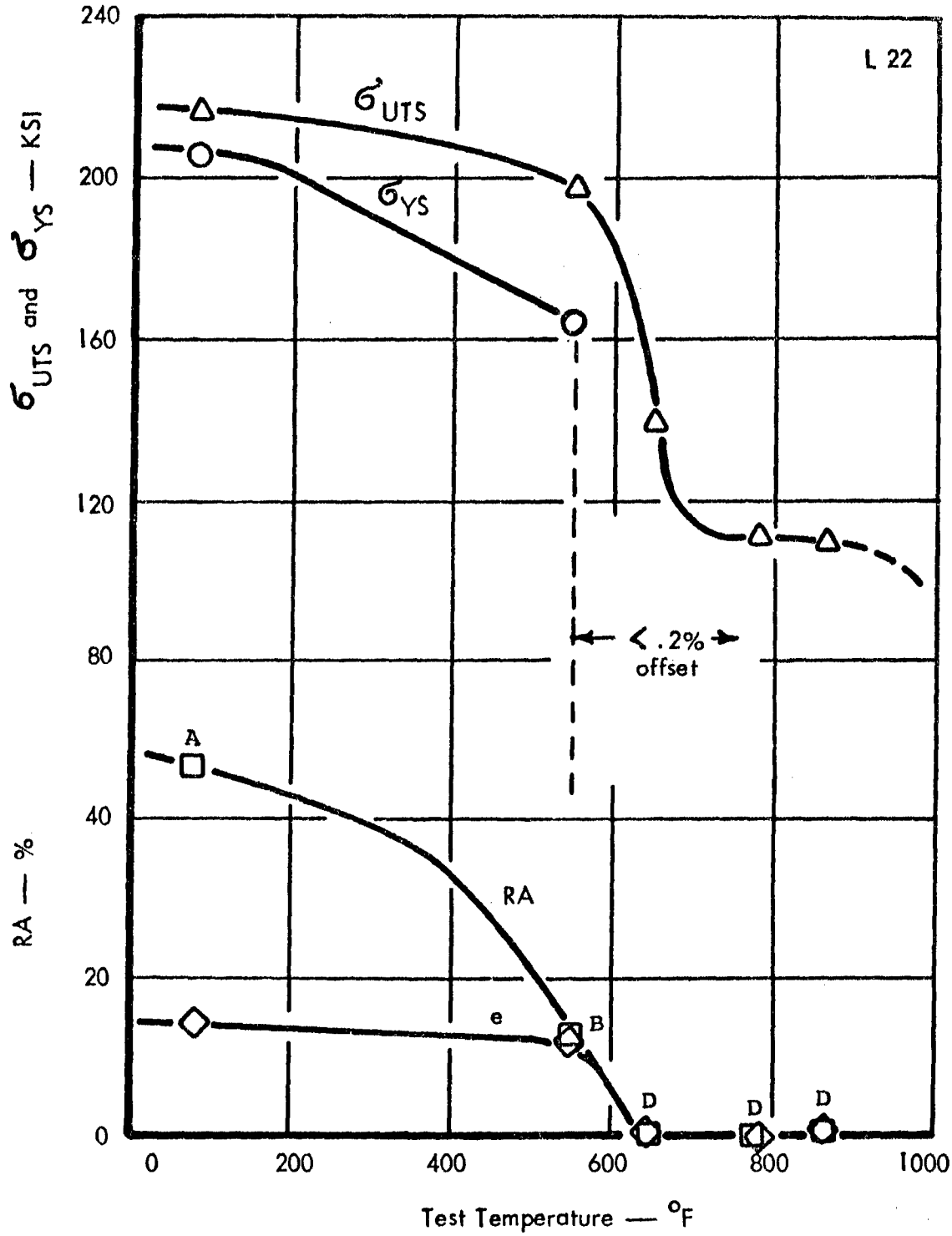

Figure 10A. Engineering Tensile Properties of Leaded L-22 Material.

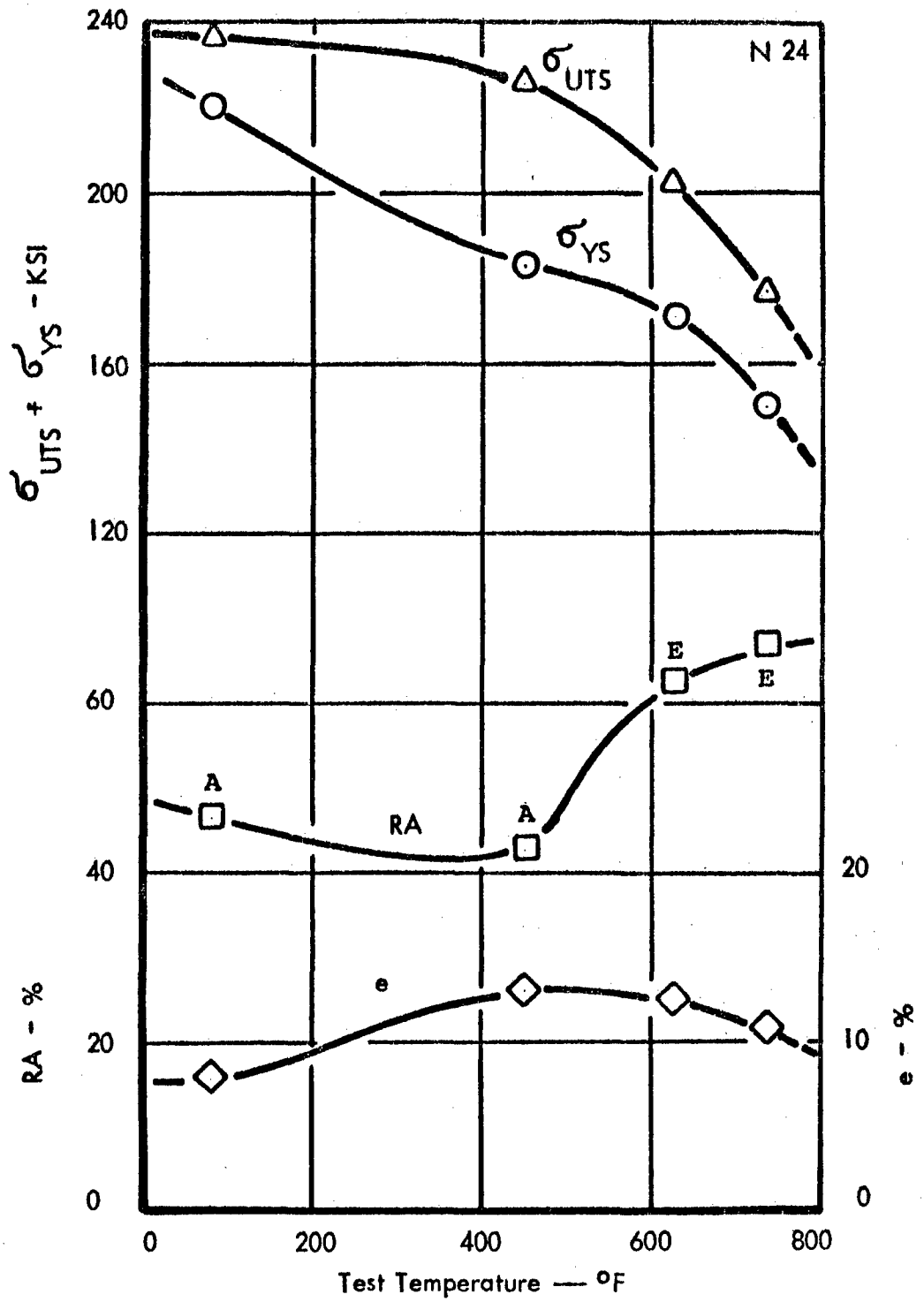

Figure 11A. Engineering Tensile Properties of Non-Leaded N-24 Material.

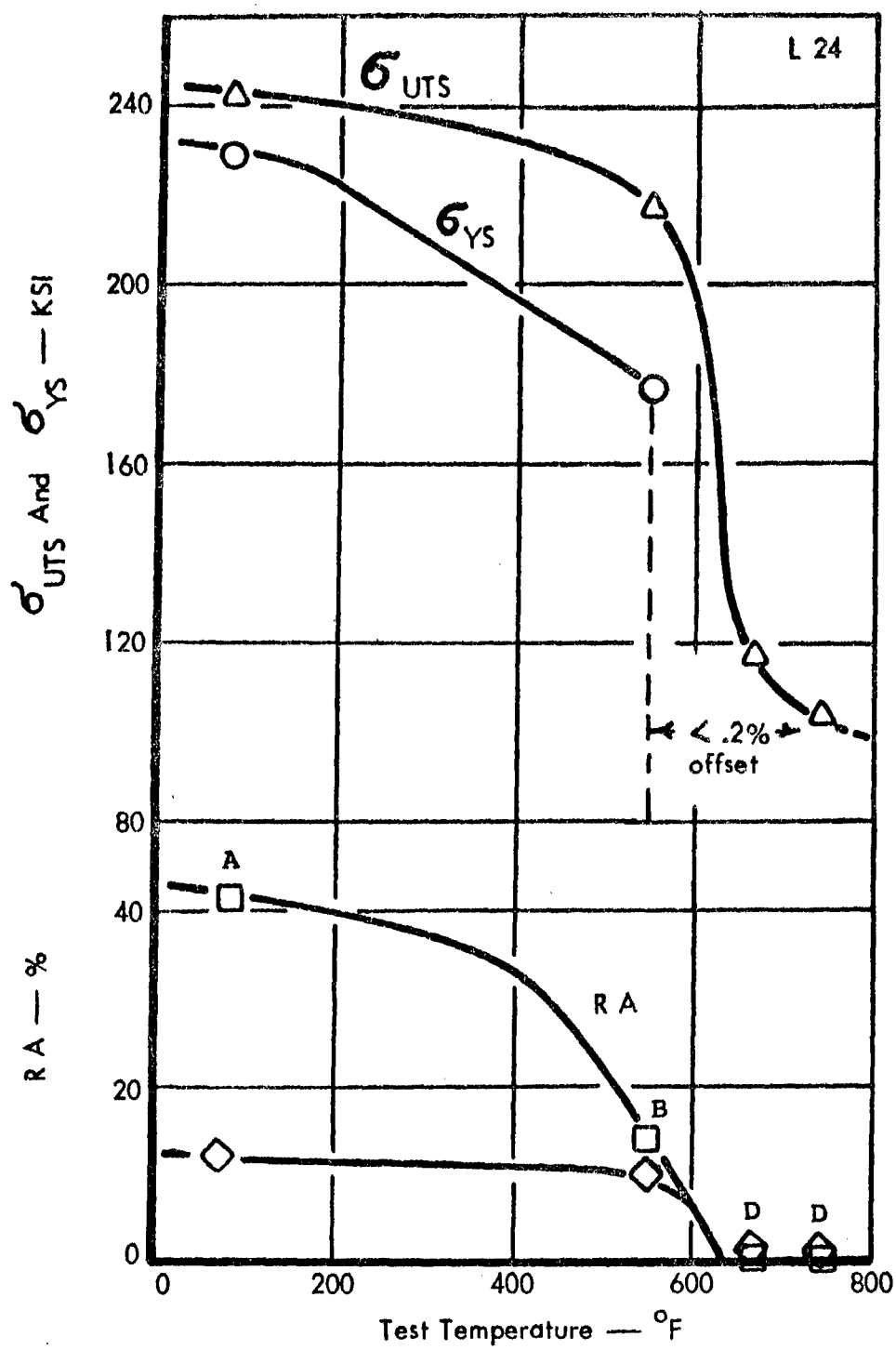

Figure 12A. Engineering Tensile Properties of Leaded L-24 Material.

APPENDIX B

PROBE WORK

Electron probe work was performed on leaded 4145 steel by John Vettraino at TACOM (Detroit Arsenal). Figure 1B shows the presence of an inclusion that was detected by using back scattered electrons. The dark areas contained in the inclusion represent elements that have low atomic numbers, while the light areas represent elements that have high atomic numbers. The inclusion was scanned for manganese (Figure 2B) and the electron pattern revealed that the manganese was present in the dark central region of Figure 1B. Next, the inclusion was scanned for sulfur (Figure 3B) and the results showed that the sulfur was also present in the dark center region of Figure 1B. When the inclusion was examined for lead (Figure 4B), the resulting electron pattern revealed that the lead was located in the light tail end regions of Figure 1B. From the above analysis it can be concluded that the manganese sulfide inclusions in leaded 4145 steel are surrounded by an envelope of lead.

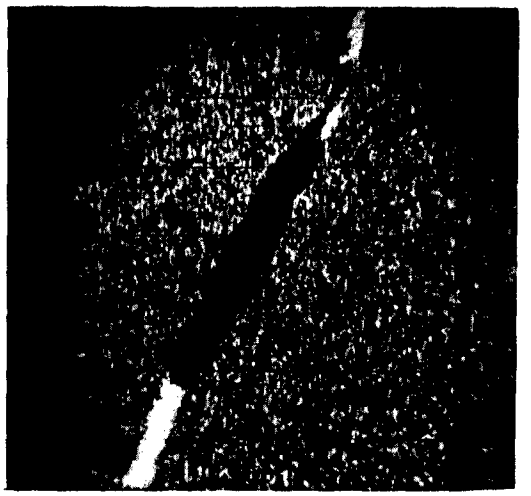

Figure 1B. Inclusion Detected by Back Scattered Electrons.

Figure 2B. Kα Radiation Revealing the Presence of Manganese in the Inclusion.

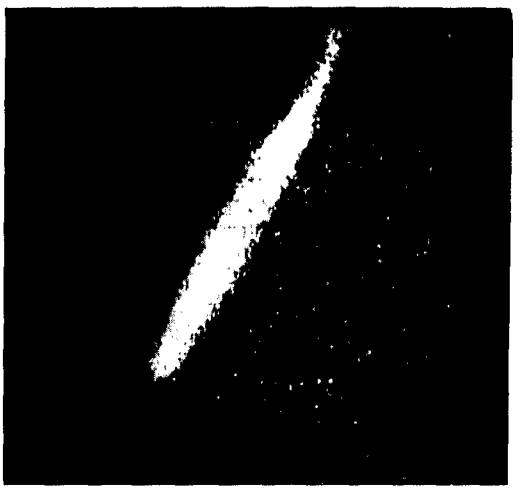

Figure 3B. Kα Radiation Revealing the Presence of Sulfur in the Inclusion.

Figure 4B. Mα Radiation Revealing the Presence of Lead in the Inclusion.

28 March, 1966

DISTRIBUTION LIST FOR REPORTS PREPARED FOR

CONTRACT DA-20-113-AMC-10820(T)

Use revised list

	No. of Copies
Commanding General U. S. Army Tank-Automotive Center Warren, Michigan 48090	
Attention: Director, Research and Engineering Directorate, SMOTA-R	1
Components Research and Development Labs, SMOTA-RC	3
Material Development and Engineering Div, SMOTA-RE	2
International Technical Programs Div, SMOTA-RI	1
Procurement Engineering Division, SMOTA-RS	2
Advanced Systems and Concepts Research Div, SMOTA-RR	2
Maintenance Directorate, SMOTA-M	2
Quality Assurance Directorate, SMOTA-Q	2
Plans and Commodity Office, SMOTA-W	2
Technical Data Coordination Branch, SMOTA-RTS	3
Combat Dev Comd Liaison Office, SMOTA-LCDC	2
Marine Corp Liaison Office, SMOTA-LMC	2
AF MIPR Liaison Office, SMOTA-USAF	2
Canadian Army Liaison Office, SMOTA-LCAN	2
USA EL Liaison Office, SMOTA-LEL	2
USA Weapons Comd Liaison Office, SMOTA-LWC	2
Reliability Engineering Branch, SMOTA-RTT	1
Sheridan Project Managers Office, AMCPM-SH-D	1
General Purpose Vehicles Project Managers Ofc, AMCPM-GP	1
M60, M60A1, M48A3 Project Managers Office, AMCPM-M60	1
Combat Veh Liaison Office, AMCPM-CV-D	1
US FRG MBT Detroit Office, AMCPM-MBT-D	1
XM561 Project Managers Office, AMCPM-GG	1
Commanding General U. S. Army Material Command Washington, D.C. Attention: AMCRD-DM-G	2
Commander Defense Documentation Center Cameron Station Alexandria, Virginia 22314	20
Harry Diamond Laboratories Washington, D. C. Attention: Technical Reports Group	1

	No. of Copies
U. S. Naval Civil Engineer Res and Engr Lab Construction Battalion Center Port Hueneme, California 93401	1
Commanding General U. S. Army Test and Evaluation Command Aberdeen Proving Ground, Maryland 21005	
Attention: AMSTE-BB	1
AMSTE-TA	1
Commanding General U. S. Army Mobility Command Warren, Michigan 48090	
Attention: AMSMO-RR	1
AMSMO-RDC	1
AMSMO-RDO	1
Commanding General U. S. Army Supply and Maintenance Command Washington, D. C. 20310	
Attention: AMSSM-MR	1
Commanding General 18th Airborne Corps Fort Bragg, North Carolina 28307	1
Commanding General U. S. Army Alaska APO 409 Seattle Washington 98100	1
Office, Chief of Research and Development Department of the Army Washington, D. C. 20000	2
U. S. Army Deputy Chief of Staff for Logistics Washington, D. C. 20000	2
U. S. Army Deputy Chief of Staff for Operations Washington, D. C.	2
Commander U. S. Marine Corps Washington, D. C. 20000	
Attention: AO-4H	1

	No. of Copies
Commanding Officer U. S. Army Aviation Material Labs Fort Eustis, Virginia Attention: TCREC-SDL	1
Commanding General U. S. Army General Equipment Test Activity Fort Lee, Virginia 23801 Attention: Transportation Logistics Test Directorate	1
Commanding General U. S. Army Medical Services Combat Developments Agency Fort Sam Houston, Texas 78234	2
Commanding Officer Signal Corps Fort Mommouth, New Jersey 07703 Attention: CSRDL	2
Commanding Officer Yuma Proving Ground Yuma, Arizona 85364 Attention: STEYP-TE	1
Corps of Engineers U. S. Army Engineer Research and Development Labs Fort Belvoir, Virginia 22060	1
President U. S. Army Maintenance Board Fort Knox, Kentucky 40121	1
President U. S. Army Armor Board Fort Knox, Kentucky 40121	1
President U. S. Army Artillery Board Fort Sill, Oklahoma 73503	1
President U. S. Army Infantry Board Fort Benning, Georgia 31905	1
President U. S. Army Airborne Electronic and Special Warfare Board Fort Bragg, North Carolina 28307	1

	No. of Copies
President U. S. Army Arctic Test Center APO Seattle, Washington 98733	1
Director, Marine Corps Landing Forces Development Center Quantico, Virginia 22134	1
Commanding Officer Aberdeen Proving Ground Aberdeen Proving Ground, Maryland 21005 Attention: STEAP-TL	1

Unclassified

Security Classification

DOCUMENT CONTROL DATA - R & D

(Security classification of title, body of abstract and indexing annotation must be entered when the overall report is classified)

1. ORIGINATING ACTIVITY *(Corporate author)* Illinois Institute of Technology Metallurgical Engineering Department Chicago, Illinois 60616	2a. REPORT SECURITY CLASSIFICATION Unclassified 2b. GROUP

3. REPORT TITLE

The Effect of Lead on Nicro-Crack Initiation and Propagation in Alloy Steels

Part B: A Fractographic Study of Leaded 4145 Steel Tested at Elevated Temperatures

4. DESCRIPTIVE NOTES *(Type of report and inclusive dates)*

Technical Report, Final Report Phase 1, Part B, August 1968

5. AUTHOR(S) *(First name, middle initial, last name)*

William R. Warke Norman N. Breyer

6. REPORT DATE August 1968	7a. TOTAL NO. OF PAGES 66	7b. NO. OF REFS 9
8a. CONTRACT OR GRANT NO. DA-20-113-AMC-10820(T) b. PROJECT NO. c. d.	9a. ORIGINATOR'S REPORT NUMBER(S) 9b. OTHER REPORT NO(S) *(Any other numbers that may be assigned this report)*	

10. DISTRIBUTION STATEMENT

Distribution of This Document is Unlimited

11. SUPPLEMENTARY NOTES	12. SPONSORING MILITARY ACTIVITY Department of the Army United States Army Tank-Automotive Command Vehicular Components and Materials Laboratory Warren, Michigan 48090

13. ABSTRACT

It has been found that a 4145 steel containing 0.3% lead suffers a loss in ductility when tensile tested between 400°F and 900°F. A visual analysis of the fractured surfaces from both leaded and non-leaded tensile specimens was performed at various ultimate strength levels from 120 KSI to 240 KSI and the fractures were classified into five types.

An electron microscope fractographic study was made on the five fracture types. Fractographs taken from Type A fractures (R.T. to 400°F) showed that fracture by microvoid coalesence ("dimpled rupture") typified the entire fracture surface. Type B fractures (400°F to 600°F) were characterized by a mixture of intergranular regions in an otherwise transgranular failure. Each group of intergranular grain facets contained an inclusion. For a Type C fracture (600°F to 650°F replicas taken from a cluster of small "fish eyes" showed both intergranular and transgranular modes of failure. Again, inclusions were present on the intergranular grain facets. A type D fracture (650°F to 900°F) was almost 100% intergranular at the origin of the single flat "fish eye." The per cent intergranular decreased as the crack grew until it was 100% transgranular near the extremity of the fracture at the far side of the "fish eye." Once again inclusions were present on the intergranular facets. Due to the fact that the Type E fracture occurs at high temperature (above 900°F), the surfaces were badly oxidized but appear to have been formed by a dimpled rupture process. The association of inclusions with the intergranular fracture regions was deemed significant since the lead was always found in an envelope surrounding the inclusions. The results of this study are compatible with a "liquid metal embrittlement" interpretation of the loss in ductility at elevated temperature.

DD FORM 1 NOV 65 1473 REPLACES DD FORM 1473, 1 JAN 64, WHICH IS OBSOLETE FOR ARMY USE.

Unclassified

Security Classification

Unclassified

Security Classification

14. KEY WORDS	LINK A ROLE	LINK A WT	LINK B ROLE	LINK B WT	LINK C ROLE	LINK C WT
Leaded Steels						
Alloy Steels						
High Strength Steels						
Embrittlement						
Liquid Metal Embrittlement						
Cracking						
Service Failures						
Processing Failures						
Fracture						
Fractography						
Elevated Temperatures						
Tensile Properties						
Design Mechanical Properties						

Unclassified

Security Classification